

Thermospheric Responses to Gravity Waves: Influences of Increasing Viscosity and Thermal Diffusivity

Sharon L. Vadas¹ and David C. Fritts

Colorado Research Associates, a division of NorthWest Research Associates
3380 Mitchell Lane, Boulder, CO

Keywords: gravity waves, viscous dissipation, thermosphere dynamics

Abstract

A gravity wave anelastic dispersion relation is derived that includes molecular viscosity and thermal diffusivity to explore the damping of high-frequency gravity waves in the thermosphere. The time dependence of the wave amplitudes and general ray-trace equations are also derived. In the special case that the thermal structure is isothermal and the Prandtl number equals one, exact linear solutions are obtained. For high-frequency gravity waves with $\omega_{Ir}/N \ll 1$, an upward-propagating gravity wave dissipates at an altitude given by $\simeq z_1 + H \ln(\omega_{Ir}/2H|m|^3\nu_1)$, where H is the density scale height, N is the buoyancy frequency, ν_1 is the viscosity at $z = z_1$, and ω_{Ir} and m are the gravity wave intrinsic frequency and vertical wavenumber, respectively. Thus, high-frequency gravity waves with large vertical wavelengths dissipate at the highest altitudes, resulting in momentum and energy inputs extending to very high altitudes. We find that the vertical wavelength of a gravity wave with an initially large vertical wavelength decreases significantly by the time it dissipates just below where it begins to reflect. The effect of diffusion on a gravity wave is similar to the effect of shear in the sense that as the molecular viscosity and thermal diffusivity increase due to decreasing background density, the intrinsic frequency plus $m\nu/H$ decreases and the vertical wavenumber increases in order to satisfy the dispersion relation for $\text{Pr} = 1$, where Pr is the Prandtl number. We also briefly explore the results with different Prandtl numbers using numerical ray-tracing. Gravity waves in a $\text{Pr} = 0.7$ environment dissipate just a few kilometers below those in a $\text{Pr} = 1$ environment when $H = 7$ km, showing the utility of the analytic, $\text{Pr} = 1$ solutions.

Submitted to JGR: November 2004

¹Corresponding author: Sharon Vadas, CoRA, 3380 Mitchell Lane, Boulder, CO, 80301, USA, W (303)415-9701x202, F (303)415-9702, vasha@co-ra.com

1. Introduction

The propagation, interactions, and dissipation of gravity waves (GWs) throughout the atmosphere are important fields of study at present. This is because GWs arising from convection, topography, wind shear, and other sources at lower altitudes transport energy and momentum from regions of higher density to regions that are more rarefied. Significant responses result in regions where these GWs dissipate, among them closure of the mesospheric jets, a cold polar summer mesopause and warm polar winter mesopause, and turbulent mixing and transport of heat, momentum, and constituents (see the recent review by Fritts and Alexander [2003]). GW propagation and effects at higher altitudes are poorly understood at present, but are likely to play similar roles in thermospheric dynamics.

There is a long history of GW observations in the thermosphere and of theories addressing various aspects of their thermospheric dynamics [e.g., Thome, 1964; Midgley and Liemohn, 1966; Hines, 1960, 1967, 1968a, b, 1973; Harris et al., 1969; Newton et al., 1969; Volland, 1969; Myers and Yanowitch, 1971; Hocke and Schlegel, 1996; Oliver et al., 1997]. While the properties of individual GWs in the thermosphere have been studied to some extent, the detailed dynamics of GW packets, their penetration altitudes, and their thermospheric effects are essentially unknown at present. Our interest here is in the potential for GW packets arising from coherent, intermittent sources (such as deep convection) to penetrate to high altitudes and to deposit significant momentum and energy as they dissipate. Depending on GW amplitudes and their penetration altitudes, such motions may play roles in both neutral and plasma processes. In particular, accelerations accompanying GW momentum flux divergence near dissipation altitudes may provide substantial forcing to the neutral atmosphere, while various researchers have suggested that GWs having suitable characteristics and amplitudes may provide the seeding mechanism for equatorial spread-F plasma bubbles [Hysell et al., 1990; Huang et al., 1993; Sekar et al., 1995; Huang and Kelley, 1996a, b, c; Sekar and Kelley, 1998].

In a previous effort employing ray-tracing methods, Vadas and Fritts (2004) examined the dissipation of GWs arising from mesoscale convective complexes due to molecular viscosity in the thermosphere. However, the derivation for the equations used was not provided in that study. In addition, thermal diffusivity is expected to play a similar

dissipative role [Pitteway and Hines, 1963]. In this paper, we derive the dispersion relation and GW damping rate from both kinematic viscosity and thermal diffusivity. The expressions utilized in Vadas and Fritts [2004] are a special example of this derivation. We organize our paper as follows. The derivation of the anelastic dispersion relation with kinematic viscosity and thermal diffusivity and our ray-tracing methodology are described in Section 2. Section 3 presents the GW solution in a viscous and diffusive, Boussinesq fluid. Sections 4 and 5 provide analytic, anelastic solutions that result when $\text{Pr} = 1$ and for special cases. Numerical results obtained via ray-tracing are presented in Section 6. Section 7 provides a brief discussion of the influence of increasing thermospheric temperatures on the GW dissipation altitude. Our summary and conclusions are presented in Section 8.

2. Gravity wave propagation and dissipation

The propagation of GWs in an anelastic fluid that has negligible viscosity and thermal diffusivity and for which the Coriolis torque is negligible, can be described by the anelastic dispersion relation [Gossard and Hooke, 1975]

$$\omega_I^2 \simeq \frac{k_H^2 N^2}{m^2 + k_H^2 + 1/4H^2}, \quad (1)$$

where N is the buoyancy frequency, k , l , and m are the zonal, meridional, and vertical wavenumbers, respectively, $k_H^2 = k^2 + l^2$, H is the density scale height, and ω_I is the intrinsic wave frequency. Eq. (1) accurately represents the structure and behavior of the highest-frequency GWs in the mesosphere. As these waves propagate above the turbopause (located at approximately 110 km), however, GW damping from molecular diffusion and thermal diffusivity become increasingly important due to the decreasing background density. These processes are highly dependent on a GW's parameters; GWs with larger vertical wavelengths and vertical group velocities propagate higher into the thermosphere before dissipating than GWs with smaller vertical wavelengths and vertical group velocities. Consequently, the dispersion relation must be modified to account for the role of dissipation in defining wave structure and propagation. We neglect ion drag, as it will not significantly affect the higher-frequency GWs of greatest interest here (i.e. having periods less than one hour [Gossard and Hooke, 1975, p241]). We also neglect wave-induced diffusion, because it will not significantly diffuse high-frequency,

large vertical wavelength GWs of greatest interest here [Del Genio and G. Schubert, 1979].

In a previous paper, we examined the dissipation of gravity waves subjected only to molecular viscosity (Vadas and Fritts, 2004). That work described only part of the thermospheric damping, however, because the Prandtl number throughout the mesosphere and lower thermosphere is approximately 0.7 [Kundu, 1990], suggesting similar damping rates from kinematic viscosity and thermal diffusivity. Here we include both molecular viscosity and thermal diffusivity, which represent a more complete description of the dissipation processes affecting high-frequency GWs in the thermosphere.

a. General dispersion relation

In order to take into account the appropriate diffusion processes for high-frequency GWs in the thermosphere, we start with the nonlinear, compressible fluid equations with molecular viscosity and thermal diffusivity:

$$\frac{D\mathbf{v}}{Dt} = -\frac{1}{\rho}\nabla p + \mathbf{g} + \frac{\mu}{\rho} \left[\nabla^2 \mathbf{v}' + \frac{1}{3}\nabla(\nabla \cdot \mathbf{v}') \right] \quad (2)$$

$$\frac{D\theta}{Dt} = \frac{h\theta}{C_p\rho T} \nabla^2 T' \quad (3)$$

$$\frac{D\rho}{Dt} = -\rho\nabla \cdot \mathbf{v} \quad (4)$$

where μ is molecular viscosity, h is thermal conductivity, \mathbf{v} is the velocity vector, θ is potential temperature, p is pressure, ρ is density, T is temperature, \mathbf{g} is gravitational acceleration, C_p is heat capacity at constant pressure, $D/Dt = \partial/\partial t + \mathbf{v} \cdot \nabla$, and primes denote perturbation quantities. We neglect the Coriolis force, since the GWs of interest here have high frequencies and large vertical group velocities and are virtually unaffected by this rotation. Since h and μ are approximately constant throughout our atmosphere, we assumed that they were constant in the momentum and heat equations, Eqs. (2)-(3), respectively. The thermal diffusivity is

$$\mathcal{K} = \frac{h}{C_p\rho} = \frac{\mu}{\text{Pr}\rho} = \frac{\nu}{\text{Pr}}, \quad (5)$$

where $\nu \equiv \mu/\rho$ is kinematic viscosity and Pr is Prandtl number. The molecular viscosity [Kundu, 1990, pg 93; Pitteway and Hines, 1963] contains two pieces, the second of which, $(1/3)\nabla(\nabla \cdot \mathbf{v}')$, is negligible with respect to $\nabla^2 \mathbf{v}'$ in an atmosphere with molecular

viscosity for GWs with $\lambda_z \ll 4\pi H$, where $\lambda_z \equiv 2\pi/|m|$ is the GW vertical wavelength (see Appendix A). Because we are interested in studying GWs in the anelastic approximation, we retain only the first viscous term here. Using

$$\theta = T \left(\frac{p_s}{p} \right)^{R/C_p}, \quad (6)$$

where p_s is standard pressure, and the ideal gas law, $p = R\rho T$, we eliminate p and θ from Eqs. (2)-(3) to obtain

$$\frac{D\mathbf{v}}{Dt} = -\frac{RT}{\rho} \nabla \rho - R \nabla T + \mathbf{g} + \nu \nabla^2 \mathbf{v}' \quad (7)$$

$$\frac{DT}{Dt} = -(\gamma - 1)T \nabla \cdot \mathbf{v} + \frac{\gamma \nu}{\text{Pr}} \nabla^2 T', \quad (8)$$

where $\gamma/(\gamma - 1) \equiv C_p/R$. By orienting our horizontal axis along a GW's direction of propagation, we can solve the fluid equations in 2D. The resulting dispersion relation can then be trivially generalized to 3D to account for GWs that propagate in other directions.

We set

$$u = U + u' \quad (9)$$

$$w = w' \quad (10)$$

$$T = \bar{T} + T' \quad (11)$$

$$\rho = \bar{\rho} + \rho', \quad (12)$$

where u and w are horizontal and vertical velocities, overlines denote unperturbed values, and U is the mean wind along the direction of GW propagation. For purposes of deriving the dispersion relation, we assume that the mean wind and temperature are locally constant, and vary slowly with altitude and horizontal location. We later allow the mean wind and temperature to change slowly with location when ray-tracing. We also neglect the earth's curvature and set $\mathbf{g} = -g\hat{z}$ because we are only interested in high-frequency waves that propagate rapidly vertically with only weak horizontal dispersion. Linearizing, Eqs. (7)-(8) and (4) become

$$u'_t = -RT'_x - \frac{c_s^2}{\gamma \bar{\rho}} \rho'_x + \nu \nabla^2 u' \quad (13)$$

$$w'_t = -RT'_z - \frac{c_s^2}{\gamma \bar{\rho}} \rho'_z + \frac{c_s^2}{\gamma H} \left(\frac{T'}{\bar{T}} - \frac{\rho'}{\bar{\rho}} \right) + \nu \nabla^2 w' \quad (14)$$

$$T'_t = -(\gamma - 1)\bar{T}(u'_x + w'_z) + \frac{\gamma\nu}{\text{Pr}}\nabla^2 T' \quad (15)$$

$$\rho'_t = \frac{\bar{\rho}}{H}w' - \bar{\rho}(u'_x + w'_z), \quad (16)$$

where the local scale height H is defined as $d\bar{\rho}/dz \equiv -\bar{\rho}/H$ and the local speed of sound is $c_s \equiv \sqrt{\gamma R\bar{T}}$. In addition, the subscripts t , x , and z represent $\partial/\partial t + U\partial/\partial x$, $\partial/\partial x$, and $\partial/\partial z$, respectively.

We then factor out a GW's increasing amplitude with height due to the decreasing background density following Pitteway and Hines [1963]:

$$\begin{aligned} \tilde{u} &= \left(\frac{\bar{\rho}}{\rho_0}\right)^{1/2} u', & \tilde{w} &= \left(\frac{\bar{\rho}}{\rho_0}\right)^{1/2} w', \\ \tilde{T} &= \left(\frac{\bar{\rho}}{\rho_0}\right)^{1/2} T', & \tilde{\rho} &= \left(\frac{\rho_0}{\bar{\rho}}\right)^{1/2} \rho', \end{aligned} \quad (17)$$

where ρ_0 is the density at the ground. We also assume solutions of the form

$$\tilde{u} = \tilde{u}_0 \exp[i(kx + mz - \omega t)], \quad (18)$$

etc., for \tilde{u} , \tilde{w} , $\tilde{\rho}$, and \tilde{T} in Eqs. (13)-(16). Here ω is the wave frequency with respect to the ground. In order to solve this problem analytically, all coefficients in Eqs. (13)-(16) must be locally constant. We thus must assume that the kinematic viscosity, ν , is approximately locally constant, and varies *slowly enough* over a GW vertical wavelength. Since $(d\nu/dz)/\nu \simeq H^{-1}$ and since $(d\tilde{u}/dz)/\tilde{u} \simeq m$, etc., this assumption is satisfied for GWs with vertical wavelengths smaller than $\lambda_z \lesssim 2\pi H$. The exact solution to Eqs. (13)-(16) with non-constant coefficients can only be obtained numerically. Comparisons of our solutions with the exact numerical solutions are being investigated.

Solving and generalizing to 3D by substituting $k_H^2 = k^2 + l^2$ for k^2 and $\omega - kU - lV$ for $\omega - kU$, where the unperturbed horizontal wind is $(U, V, 0)$, we obtain the compressible, complex, dispersion relation of acoustic GWs damped by both molecular viscosity and thermal diffusivity:

$$- \frac{\omega_I^2}{c_s^2} (\omega_I - i\alpha\nu)^2 \left(1 - \frac{i\gamma\alpha\nu}{\text{Pr}\omega_I}\right) + (\omega_I - i\alpha\nu) \left(\omega_I - \frac{i\alpha\nu}{\text{Pr}}\right) \left(\mathbf{k}^2 + \frac{1}{4H^2}\right) = k_H^2 N^2, \quad (19)$$

where $\mathbf{k}^2 = k_H^2 + m^2$, the intrinsic frequency is

$$\omega_I = \omega - kU - lV, \quad (20)$$

$N^2 \equiv (g/\bar{\theta}) d\bar{\theta}/dz = (\gamma - 1)c_s^2/\gamma^2 H^2$, and

$$\alpha \equiv -\mathbf{k}^2 + \frac{1}{4H^2} + \frac{im}{H}. \quad (21)$$

The corresponding polarization relations are given in Appendix B. This complex dispersion relation differs from the modified dispersion relation derived by Pitteway and Hines [1963] for two important reasons. First, they assumed that μ decreased exponentially with height in order to ensure that ν be exactly constant with height, which brought in vertical derivatives of μ . On the other hand, we set μ to be constant, and seek solutions for GWs with small enough λ_z such that $\nu = \mu/\bar{\rho}$ can be taken to be locally constant. Second, they retained the $(1/3)|\nu\nabla(\nabla\cdot\mathbf{v}')|$ molecular viscosity term because they were interested in the damping of acoustic-gravity waves, which also adds extra terms in the dispersion relation. In the limit that the molecular viscosity and thermal diffusivity are negligible, the dispersion relation becomes

$$-\frac{\omega_I^4}{c_s^2} + \omega_I^2 \left(\mathbf{k}^2 + \frac{1}{4H^2} \right) = k_H^2 N^2, \quad (22)$$

the usual compressible dispersion relation for acoustic-gravity waves [Hines, 1960].

In order to exclude the complications of acoustic waves, we neglect terms of order $(\omega_I/c_s)^2$ as compared to $(\mathbf{k}^2 + 1/4H^2)$ in Eq. (19). This yields the desired anelastic dispersion relation for GWs under the influence of molecular viscosity and thermal diffusivity:

$$(\omega_I - i\alpha\nu) \left(\omega_I - \frac{i\alpha\nu}{\text{Pr}} \right) = \frac{k_H^2 N^2}{\mathbf{k}^2 + 1/4H^2}. \quad (23)$$

If molecular viscosity only is present, the LHS (left-hand-side) of Eq. (23) is $\omega_I(\omega_I - i\alpha\nu)$. And if only thermal diffusivity is present, the LHS of Eq. (23) is $\omega_I(\omega_I - i\alpha\nu/\text{Pr})$ instead. Therefore, the effect due to thermal diffusivity alone is the same as that due to molecular viscosity alone, apart from being larger by $1/\text{Pr}$, as noted previously [Pitteway and Hines, 1963]. However, the combination of the two effects does not lead to a simple, mathematical rescaling of the molecular viscosity from ν to $\nu(1 + \text{Pr}^{-1})$ because of the presence of the extra term $-\alpha^2\nu^2/\text{Pr}$ in Eq. (23). However, for $\text{Pr} = 1$ and for high-frequency GWs with $m^2 \gg 1/4H^2$, the extra term is negligible up to and at the dissipation altitude (see Sec. 5d). Where the molecular viscosity and thermal diffusivity are negligible

at lower altitudes, Eq. (23) becomes the well-known anelastic dispersion relation for freely propagating, high-frequency, internal GWs, Eq. (1).

In the classic formulation of the dissipation of internal GWs by molecular viscosity and thermal diffusivity, Pitteway and Hines [1963] assumed a complex vertical wave number. This ansatz results in altitude-decaying wave amplitudes. For the case of constant μ , Pitteway and Hines [1963] used a lowest-order perturbation analysis with the kinematic viscosity taken to be a small quantity. Because viscosity increases with altitude, their solutions are therefore only valid up to the altitude at which dissipation is non-negligible. And the neglect of the nonlinear terms in this perturbation expansion yields good results only for waves with $\lambda_z < H$ [Midgley and Liemohn, 1966, see also Hines, 1973].

If we also assume a complex vertical wavenumber in Eq. (23), we cannot solve for the real and imaginary pieces in general. However, if we instead incorporate a complex intrinsic frequency (and a real vertical wavenumber) into the dispersion relation, resulting instead in time-decaying wave amplitudes, we can determine the solution for any value of viscosity and thermal diffusivity, and so describe the path a GW takes before, during, and after dissipation. Therefore, we allow a GW's amplitude to decay explicitly in time (and implicitly in altitude) rather than explicitly in altitude (and implicitly in time). For a GW with small λ_z which satisfies the Boussinesq approximation, we show in Section 3 that the dispersion relation and dissipation altitudes are identical when the GW's amplitude is assumed to decay explicitly in time or explicitly in altitude.

In keeping with our solution ansatz that wave amplitudes decay with time, we express the intrinsic frequency as a sum of real and imaginary parts:

$$\omega_I = \omega_{Ir} + i\omega_{Ii}. \quad (24)$$

Here, ω_{Ir} is real and relates the intrinsic GW frequency to the wave structure, buoyancy frequency, and damping due to kinematic viscosity and thermal diffusivity, and ω_{Ii} is real and expresses the inverse decay rate of the wave amplitude with time due to kinematic viscosity and thermal diffusivity. (The inverse decay rate of the wave momentum flux is approximately twice ω_{Ii}). Comparing Eqs. (20) and (24) implies that there is an imaginary component of ω even at ground level, although it is negligible because the molecular viscosity and thermal diffusivity are extremely small there.

Substituting Eq. (24) into Eq. (23), we obtain the inverse decay rate,

$$\omega_{Ii} = -\frac{\nu}{2} \left(\mathbf{k}^2 - \frac{1}{4H^2} \right) \frac{[1 + (1 + 2\delta)/\text{Pr}]}{(1 + \delta_+/2)}, \quad (25)$$

as well as the GW dispersion relation,

$$\begin{aligned} \omega_{Ir}^2 + \frac{\nu^2}{4} \left(\mathbf{k}^2 - \frac{1}{4H^2} \right)^2 (1 - \text{Pr}^{-1})^2 \frac{(1 + \delta_+ + \delta^2/\text{Pr})}{(1 + \delta_+/2)^2} + \frac{\nu_+ m \omega_{Ir}}{H} + \frac{\nu^2 m^2}{\text{Pr} H^2} \\ = \frac{k_H^2 N^2}{\mathbf{k}^2 + 1/4H^2}, \end{aligned} \quad (26)$$

where $\delta_+ = \delta(1 + \text{Pr}^{-1})$, $\nu_+ = \nu(1 + \text{Pr}^{-1})$, and $\delta = \nu m/H\omega_{Ir}$. This dispersion relation is nonhydrostatic and compressible, but excludes acoustic waves, similar to Marks and Eckermann [1995]. In the limit that molecular viscosity and thermal diffusivity are negligible in the stratosphere and mesosphere, the damping rate is zero ($\omega_{Ii} = 0$), $|\delta| \ll 1$ and $|\delta_+| \ll 1$, and GWs propagate with the usual dispersion relation, Eq. (1). Eqs. (38)-(39) of Vadas and Fritts (2004) can be easily obtained from Eqs. (25)-(26) by setting $\text{Pr} = \infty$ (i.e., no thermal diffusivity).

b. Ray-tracing methodology

If a GW packet is propagating in a background wind of $\mathbf{V}(\mathbf{x}) = (V_1, V_2, V_3) = (U, V, W)$, then its evolution in space and time is [Lighthill, 1978]

$$\frac{dx_i}{dt} = V_i + \frac{\partial \omega_{Ir}}{\partial k_i} = V_i + c_{gi}, \quad (27)$$

$$\frac{dk_i}{dt} = -k_j \frac{\partial V_j}{\partial x_i} - \frac{\partial \omega_{Ir}}{\partial x_i}, \quad (28)$$

where the indices $i, j = 1, 2, 3$ indicate the components of the vector quantities \mathbf{x} , \mathbf{V} , \mathbf{k} , and the group velocity \mathbf{c}_g . Additionally, repeated indices imply a summation, $\omega_{Ir} = \omega_r - kU - lV$, and ω_r is the real part of the ground-based frequency ω .

Due to its inherent complexity, the GW dispersion relation, Eq. (26), cannot be solved analytically for ω_{Ir} in general. However, this is not necessary for the purposes of ray-tracing, since the intrinsic frequency can be determined at any location by evaluating $\omega_{Ir} = \omega_r - kU - lV$, since ω_r remains constant along a ray's path provided the unperturbed background variables are independent of time [Lighthill, 1978]. The derivatives $\partial \omega_{Ir}/\partial k$, $\partial \omega_{Ir}/\partial l$, $\partial \omega_{Ir}/\partial m$, and $\partial \omega_{Ir}/\partial x_i$ are given by Eqs. (C.1)-(C.4) in Appendix C.

In general applications, $N(z)$, $H(z)$, $\bar{\theta}(z)$, and $\nu(z) = \mu/\bar{\rho}(z)$ all vary with altitude, latitude, season, and the presence of large-scale wave structures. As in Vadas and Fritts (2004), we examine the dissipation of GWs in an isothermal atmosphere for simplicity. We set $\mu = 0.017 \text{ gm m}^{-1} \text{ s}^{-1}$, $N_0 = 0.02 \text{ rad s}^{-1}$, $H_0 = 7.0 \text{ km}$, $\bar{T}_0 = 250 \text{ K}$, $\text{Pr} = 0.7$, $\gamma = 1.4$, $z_0 = 0$, and $\bar{\rho}_0 = 10^3 \text{ gm m}^{-3}$. This yields a kinematic viscosity at 90 km of $\nu = \mu/\bar{\rho} = 6.5 \text{ m}^2 \text{ s}^{-1}$, which is similar to the value used by Pitteway and Hines [1963]. To achieve accurate numerical solutions, a 4th-order Runge Kutta routine [Press et al., 1992] is employed to advance the ray equations in time.

3. Damping in a Boussinesq fluid

a. Damping from viscosity only

In order to compare the GW dispersion relation and dissipation altitude when employing the time-decaying and altitude-decaying assumptions, we first consider the simple example of a small λ_z GW satisfying the Boussinesq approximation, and experiencing only molecular viscosity. Setting $H \rightarrow \infty$ and $\text{Pr} \rightarrow \infty$, Eq. (23) becomes

$$\mathbf{k}^2 \omega_I^2 + i\nu \mathbf{k}^4 \omega_I = k_H^2 N^2. \quad (29)$$

a.1 Decay of wave amplitudes with time

If we assume that the GW amplitudes decay explicitly in time (and implicitly in altitude), then the intrinsic frequency ω_I is complex and the vertical wavenumber m is real. Substituting Eq. (24) into Eq. (29), we obtain

$$\omega_{Ii} = -\frac{\nu \mathbf{k}^2}{2} \quad (30)$$

$$\omega_{Ir}^2 = \frac{k_H^2 N^2}{\mathbf{k}^2} - \frac{\nu^2 \mathbf{k}^4}{4}. \quad (31)$$

To first order in ν , the GW dispersion relation is unaffected by viscosity and the attenuation is linearly proportional to ν . Using Eqs. (27)-(28), the ray equations are

$$\frac{dz}{dt} = \frac{\partial \omega_{Ir}}{\partial m} = -\frac{m}{\omega_{Ir}} \left(\frac{k_H^2 N^2}{\mathbf{k}^4} + \frac{\nu^2 \mathbf{k}^2}{2} \right) \quad (32)$$

$$\frac{dm}{dt} = -\frac{\partial \omega_{Ir}}{\partial z} = \frac{\nu \mathbf{k}^4}{4 \omega_{Ir}} \frac{d\nu}{dz}. \quad (33)$$

Because ν is positive and increases rapidly with altitude, $dm/dt > 0$. Since $m < 0$ for an upward propagating GW, $|m|$ decreases (or λ_z increases) until the GW eventually

reaches the altitude where $m = 0$. There, $dz/dt = 0$ from Eq. (32), and the GW reflects downwards at its turning or “reflecting altitude”.

When a GW dissipates, momentum flux divergence occurs, and a body forcing arises. We define the dissipation altitude to be the altitude where the GW momentum flux (per unit mass) is a maximum. As shown in Section 3c, the dissipation altitude occurs at the altitude where the inverse of the dissipative decay rate equals the time taken for a GW to propagate vertically by two scale heights. This occurs when $2\omega_{Ir}H/c_{gz} \simeq -1$ (see Eq. (54)). Since $c_{gz} \simeq -m\omega_{Ir}/\mathbf{k}^2$, the dissipation altitude occurs where

$$\frac{H\nu_{\text{diss}}\mathbf{k}^4}{|m|\omega_{Ir}} \simeq 1, \quad (34)$$

where we have used Eq. (30). For example, in an isothermal atmosphere with $H = 7$ km, a GW with $\lambda_z = 5$ km and $\omega_{Ir} = 0.005$ rad s⁻¹ dissipates at $z \simeq 118$ km. The maximum body force induced by this wave occurs $\ln(2)H \simeq 5$ km higher in altitude in this example (see Eq. (55)).

At the dissipation altitude, $\nu_{\text{diss}}^2\mathbf{k}^4/4 = \omega_{Ir}^2(m^4/\mathbf{k}^4)/4H^2m^2$, which is much smaller than ω_{Ir}^2 for high frequency GWs with vertical wavelengths limited by $\lambda_z \ll 4\pi H$. Combining this result with Eq. (31), the dispersion relation is not significantly altered by viscosity at the dissipation altitude for small λ_z GWs (which satisfy the Boussinesq approximation), and therefore their vertical wavelengths will not change significantly by the time they dissipate. Therefore, at the higher altitude range where these GWs eventually reflect, their momentum flux will have already decreased to negligible values. This will be verified later via numerical ray-tracing (see Fig. 2a, 3).

a.2 Decay of wave amplitudes with altitude

If we now assume that the GW amplitudes decay explicitly in altitude (and implicitly in time), the vertical wavenumber m is complex and the intrinsic frequency ω_I is real. We set

$$m = m_r + im_i \quad (35)$$

$$m^2 = M^2 + i\beta, \quad (36)$$

where m_r and im_i are the real and imaginary components of the vertical wavenumber, respectively, and m_i is the inverse dissipation scale of the wave amplitude. In addition,

$M^2 \equiv m_r^2 - m_i^2$ and $\beta \equiv 2m_r m_i$ are real. Substituting Eq. (36) into Eq. (29), the GW dispersion relation becomes

$$\omega_I^4 + 4\nu^2 \mathbf{K}^4 \omega_I^2 = \frac{k_H^4 N^4}{\mathbf{K}^4}, \quad (37)$$

where $\mathbf{K}^2 = k_H^2 + M^2$. As before, if an upgoing GW propagates through a constant background wind, ω_I remains constant. The solutions are $m_i = \beta/2m_r$,

$$\mathbf{K}^4 = -\frac{\omega_I^2}{8\nu^2} + \sqrt{\frac{\omega_I^4}{64\nu^4} + \frac{k_H^4 N^4}{4\nu^2 \omega_I^2}} \quad (38)$$

$$\beta = \frac{\mathbf{K}^2 \omega_I^2 - k_H^2 N^2}{2\nu \omega_I \mathbf{K}^2} \quad (39)$$

$$m_r^2 = \frac{1}{2}(\mathbf{K}^2 - k_H^2) + \frac{1}{2}\sqrt{(\mathbf{K}^2 - k_H^2)^2 + \beta^2}. \quad (40)$$

In the limit that $\nu \mathbf{k}^2/\omega_I \ll 1$, $\omega_I^2/N^2 \ll 1$ and $m_r^2 \gg k_H^2$, to lowest order in ν , the GW dispersion relation is $m_r^2 \simeq k_H^2 N^2/\omega_I^2 + \mathcal{O}(\nu^2)$, and the inverse dissipation scale is

$$m_i \simeq -\frac{\nu m_r^3}{2\omega_I}. \quad (41)$$

The dissipation altitude occurs where $m_i H \simeq -1/2$ (see Eq. (56)), or

$$\frac{\nu_{\text{diss}} m_r^3 H}{\omega_I} \simeq 1. \quad (42)$$

This result is identical to that obtained previously for the time-varying ansatz, Eq. (34), when $m_r^2 \gg k_H^2$. In deriving this result, we assumed that $\nu \mathbf{k}^2/\omega_I \ll 1$. Using Eq. (42), at the dissipation altitude and for waves with $m_r^2 \gg k_H^2$, then $\nu_{\text{diss}} \mathbf{k}^2/\omega_I \simeq \lambda_z/2\pi H$. This quantity is much less than one when $\lambda_z \ll 2\pi H$. Because the dispersion relation is $m_r^2 \simeq k_H^2 N^2/\omega_I^2$ to lowest order in ν , m is not significantly changed at the dissipation altitude, as also found for the time-varying ansatz. Therefore, the assumption $\nu \mathbf{k}^2/\omega_I \ll 1$ is valid for GWs satisfying the Boussinesq approximation. In addition, the dissipation altitude and the GW dispersion relation at and below the dissipation altitude are the same for the time and space varying amplitude ansatzs.

b. Damping from viscosity and thermal diffusivity

We now generalize the dissipation to include both molecular viscosity and thermal diffusivity. Making the approximations $H \rightarrow \infty$ and $\text{Pr} = 1$ in Eq. (23), the complex dispersion relation of a viscous, Boussinesq fluid is

$$\mathbf{k}^2 \omega_I^2 + i2\nu \mathbf{k}^4 \omega_I - \nu^2 \mathbf{k}^6 = k_H^2 N^2. \quad (43)$$

b.1 Decay of wave amplitudes with time

Assuming that GW amplitudes decay explicitly with time, the inverse decay rate in time of the wave amplitude and the GW dispersion relation are (see Eqs. (25)-(26))

$$\omega_{Ii} = -\nu \mathbf{k}^2 \quad (44)$$

$$\omega_{Ir}^2 = \frac{k_H^2 N^2}{\mathbf{k}^2}. \quad (45)$$

Comparing Eq. (44) to Eq. (30), the damping rate here is twice as large, and the estimated dissipation altitude is $0.7H$ lower (in an isothermal atmosphere). Unlike for the $\text{Pr} = \infty$ example in Section 3.a.1, however, the wave dispersion relation is unaffected by viscosity, so that $dm/dt = 0$ and m does not change with altitude.

b.2 Decay of wave amplitudes with altitude

Assuming instead that the wave amplitudes decay explicitly with altitude, and taking ν to lowest order, the complex GW dispersion relation is

$$\mathbf{k}^2 \omega_I^2 + i2\nu \mathbf{k}^4 \omega_I \simeq k_H^2 N^2. \quad (46)$$

This is identical to Eq. (29) but with twice the viscosity. Using the results of Section 3.a.2 but replacing $\nu \rightarrow 2\nu$, the inverse dissipation scale is

$$m_i \simeq -\frac{\nu m_r^3}{\omega_I}. \quad (47)$$

for $\omega_I^2/N^2 \ll 1$ and $m_r^2 \gg k_H^2$ to lowest order in ν . Comparing with Eq. (41), the dissipation scale is one-half as large here, as expected, leading to a dissipation altitude $0.7H$ lower in altitude.

In summary, the time and altitude varying assumptions lead to identical dissipation altitudes and dispersion relations at and below the dissipation altitudes in the Boussinesq approximation, lending credibility to the idea that the same must also be true in the

anelastic approximation. We also found that including thermal diffusivity with $\text{Pr} = 1$ leads to the same solutions but with twice the viscosity and with dissipation altitudes $0.7H$ lower.

c. Momentum fluxes and body forcings

As a GW propagates upwards, its perturbation velocity increases with altitude as $1/\sqrt{\bar{\rho}}$ (see Eq. (17)) and decreases as $\exp(\omega_{Ii}t)$ in time due to dissipation (assuming ω_I complex and m real). Putting these two effects together, the momentum flux of a GW per unit mass (assuming no wave reflection) is

$$\overline{u'w'}(z) = \overline{u'w'}(z_1) \frac{\bar{\rho}_1}{\bar{\rho}} \exp\left(2\Sigma_{t_1}^t \omega_{Ii} \Delta t\right), \quad (48)$$

where $\bar{\rho}_1 = \bar{\rho}(z_1)$, and we sum over $\omega_{Ii} \propto \nu$ because ν is not constant in time along a ray. Here, $z = z_1$ is taken to be 2 to 3 scale heights below the dissipation altitude, in order to ignore the effects of wind shears that occur lower down in altitude. Using $dz/dt = c_{gz}$ along a ray, $c_{gz} \simeq -m\omega_{Ir}/\mathbf{k}^2$ for a wave at or below its dissipation altitude, and Eqs. (30) and (44), Eq. (48) becomes

$$\overline{u'w'}(z) \simeq \overline{u'w'}(z_1) \frac{\bar{\rho}_1}{\bar{\rho}} \exp\left(-\frac{\psi \mathbf{k}^4 \mu}{|m|\omega_{Ir}} \int_{z_1}^z \frac{dz}{\bar{\rho}}\right), \quad (49)$$

where $\psi = 1$ and 2 for $\text{Pr} = \infty$ and $\text{Pr} = 1$, respectively, and $\omega_{Ii} = -\psi\nu\mathbf{k}^2/2$. Here, m and ω_{Ir} are the GW vertical wavenumber and intrinsic frequency at $z = z_1$. In deriving Eq. (49), we have neglected the variation with height of m above $z = z_1$, which is a good approximation for GWs satisfying the Boussinesq approximation (see Sec. 3a and Fig. 2a). We also assumed that ω_{Ir} was constant above z_1 , or that mean winds above z_1 are approximately constant. The body force resulting from a GW dissipating is

$$F_b(z) = -\frac{1}{\bar{\rho}} \frac{\partial(\bar{\rho} \overline{u'w'})}{\partial z} \quad (50)$$

$$\simeq \overline{u'w'}(z_1) \frac{\psi \mathbf{k}^4 \nu_1}{|m|\omega_{Ir}} \left(\frac{\bar{\rho}_1}{\bar{\rho}}\right)^2 \exp\left(-\frac{\psi \mathbf{k}^4 \mu}{|m|\omega_{Ir}} \int_{z_1}^z \frac{dz}{\bar{\rho}}\right), \quad (51)$$

where $\bar{\rho}_1$ and ν_1 are the values of $\bar{\rho}$ and ν at $z = z_1$, respectively.

If the atmosphere is isothermal and unsheared above z_1 , the wave momentum flux and body force profiles are

$$\overline{u'w'}(z) \simeq \overline{u'w'}(z_1) \exp\left[\frac{z - z_1}{H} - \frac{\psi H \mathbf{k}^4 \nu_1}{|m|\omega_{Ir}} \left(\exp\left(\frac{z - z_1}{H}\right) - 1\right)\right] \quad (52)$$

$$F_b(z) \simeq \overline{u'w'}(z_1) \frac{\psi \mathbf{k}^4 \nu_1}{|m| \omega_{Ir}} \exp \left[\frac{2(z - z_1)}{H} - \frac{\psi \mathbf{Hk}^4 \nu_1}{|m| \omega_{Ir}} \left(\exp \left(\frac{z - z_1}{H} \right) - 1 \right) \right]. \quad (53)$$

The momentum flux profile peaks when $\partial \overline{u'w'}/\partial z = 0$, and occurs where

$$\frac{\psi \nu \mathbf{Hk}^4}{|m| \omega_{Ir}} \simeq 1 \quad \text{or} \quad 2\omega_{Ii} \frac{H}{c_{gz}} \simeq -1. \quad (54)$$

The body force profile peaks when $\partial F_b/\partial z = 0$, and occurs where

$$\frac{\psi \nu \mathbf{Hk}^4}{2|m| \omega_{Ir}} \simeq 1 \quad \text{or} \quad \omega_{Ii} \frac{H}{c_{gz}} \simeq -1, \quad (55)$$

which is higher in altitude by $\ln(2)H \simeq 0.7H$ than the peak in the momentum flux profile. GW amplitudes are proportional to $\exp(-i\omega_I t) \propto \exp(\omega_{Ii} t) = \exp(-t/\tau)$, where $\tau = -1/\omega_{Ii}$ is the dissipation decay time. Thus, the peak momentum flux (body force) altitude is where the dissipation decay time equals the time taken for the GW to propagate two (one) scale heights in altitude.

If we had instead chosen the GW amplitude to decay with altitude (assuming m complex and ω_I real), then $2\Sigma_{t_1}^t \omega_{Ii} \Delta t$ in Eq. (48) is replaced by $2\Sigma_{t_1}^t m_i \Delta z$, and $\mathbf{k}^4/|m| \omega_{Ir}$ in Eq.(49) is replaced by $|m_r|^3/\omega_I$, where we have used Eqs. (41) and (47) and $m_i = -\psi \nu m_r^3/2\omega_I$. The momentum flux profile peaks where

$$\frac{\psi \nu \mathbf{H} |m_r|^3}{\omega_I} \simeq 1 \quad \text{or} \quad 2m_i H \simeq -1, \quad (56)$$

and the body force profile peaks where

$$\frac{\psi \nu \mathbf{H} |m_r|^3}{2\omega_I} \simeq 1 \quad \text{or} \quad m_i H \simeq -1. \quad (57)$$

As found in Sec. 3a-b, the momentum flux and body force profiles when GW amplitudes vary with time or with altitude peak at the same altitudes for a GW which satisfies the Boussinesq approximation. Thus Eq. (54) is equivalent to Eq. (56), and Eq. (55) is equivalent to Eq. (57).

4. Gravity wave propagation and dissipation when isothermal and $\text{Pr} = 1$

a. Dispersion relation

In our atmosphere, the dissipation due to thermal diffusivity is about 40% stronger than that due to molecular viscosity, since $\text{Pr} \simeq 0.7$. Cursory examination of Eq. (26), however, shows that the dispersion relation simplifies greatly when the Prandtl number

equals one. Thus, we set $\text{Pr} = 1$ and $\overline{T} = \text{constant}$ in order to solve the anelastic ray-trace equations exactly and obtain insights into the implications of kinematic viscosity and thermal diffusivity for GW structure and dissipation at high altitudes. We will compare this solution to $\text{Pr} = 0.7$ numerical solutions in Section 6.

When $\text{Pr} = 1$, the LHS of Eq. (26) is a perfect square, and the dispersion relation is simply

$$\left(\omega_{I_r} + \frac{m\nu}{H}\right)^2 = \frac{k_H^2 N^2}{\mathbf{k}^2 + 1/4H^2}. \quad (58)$$

The quantity “ $\omega_{I_r} + m\nu/H$ ” can be thought of as a generalized intrinsic frequency. This dispersion relation can be understood most easily by assuming the mean wind to be constant. Since the real part of the ground-based frequency, ω_r , remains constant along a ray’s path provided the unperturbed variables (such as the mean wind and density) are independent of time [Lighthill, 1978], and since k and l are unchanged if the unperturbed quantities such as H and ν depend only on z (see Eq. (28)), then $\omega_{I_r} = \omega_r - kU - lV$ is constant for a GW along its ray path. For a GW propagating upwards into an increasingly dissipative environment, $m\nu/H$ becomes increasingly negative, thereby decreasing the LHS of Eq. (58). Since N and H are constant, the RHS (right-hand-side) can decrease only if the GW vertical wavelength decreases. This is similar to what happens to a GW that propagates into an increasing wind (i.e., $kU > 0$) with no dissipation; the GW’s intrinsic frequency decreases, which causes its vertical wavelength to decrease. If a GW propagates into an increasing wind, then the GW encounters a critical level where the wind equals the GW phase speed, at which point the GW vertical wavelength equals zero. In the case of dissipation, however, it turns out that the GW begins to reflect downwards when its vertical wavelength is non-zero, as we will see below, with the entire reflection occurring over a range of altitudes [Yanowitch, 1967, 1969; Einaudi and Hines, 1970].

The result that GWs with large vertical wavelengths experience vertical wavelength reductions with increasing altitude (or time) will be described further below, and is a generalization of previous numerical results; Vadas and Fritts (2004) showed that a GW’s vertical wavelength had decreased at the dissipative altitude under the influence of molecular viscosity only for large vertical wavelengths. These results differ from those for GWs having small vertical wavelengths under the Boussinesq approximation (see

Section 3). Under that approximation assuming molecular viscosity only, a GW’s vertical wavelength increases to “ ∞ ” at a turning level where the GW reflects downward. (We note, however, that the Boussinesq approximation is not valid for large λ_z .) Under this approximation with equal kinematic viscosity and thermal diffusivity, a GW’s vertical wavelength remains constant and the GW does not reflect. While these Boussinesq results are quite different, they only differ *above* the dissipation altitude, at which point the wave’s momentum flux (and influence on the mean state via body forcing) is negligible. As shown in Section 3, the vertical wavelength of a high-frequency wave with a small vertical wavelength increases only slightly by the time it dissipates.

b. Anelastic solution

To explore GW structure at high altitudes more fully, we assume $\text{Pr} = 1$ and locally constant U , N , and H at the GW dissipation altitude. Then $\omega_{Ir} = \text{constant}$. Using Eq. (25), the inverse decay rate of the wave amplitude is

$$\omega_{Ii} = -\nu \left(\mathbf{k}^2 - \frac{1}{4H^2} \right). \quad (59)$$

From Eq. (58) and Eqs. (27)-(28), the ray-trace equations are

$$\frac{dx}{dt} = c_{gx} + U = \frac{k(m^2 + 1/4H^2)(\omega_{Ir} + m\nu/H)^3}{k_H^4 N^2} + U \quad (60)$$

$$\frac{dz}{dt} = c_{gz} = -\frac{m(\omega_{Ir} + m\nu/H)^3}{k_H^2 N^2} - \frac{\nu}{H} \quad (61)$$

$$\frac{dm}{dt} = -\frac{\partial \omega_{Ir}}{\partial z} = \frac{m}{H} \frac{d\nu}{dz} = \frac{m\nu}{H^2}. \quad (62)$$

From Eq. (62), the change in GW vertical wavelength with altitude depends on the gradient of the kinematic viscosity rather than on the kinematic viscosity itself. Therefore in an atmosphere with constant kinematic viscosity, λ_z will not change, even though the GW is dissipating (see Eq. (59)). For an upward propagating GW, $m < 0$ so that the first term on the RHS of Eq. (61) is positive at lower altitudes, while the second term is increasingly negative with increasing altitude. Eventually, the second term equals the first, and the GWs “reflects” downwards where $dz/dt = 0$. (See Sec. 6 for a more complete discussion of GW reflection and the applicability of the WKB approximation.)

This occurs when

$$-\frac{m^2 \omega_{Ir}^2 (1 + \delta)^3}{k_H^2 N^2} = \delta, \quad (63)$$

where $\delta = m\nu/\omega_{Ir}H$ as before. At the reflection altitude, m does not equal zero as it does in the Boussinesq example. Instead, it increases as dissipation becomes more important, before the WKB approximation fails. It is unlikely that m will change sign during the short duration in time when the single wave assumption inherent in the WKB approximation is not valid and the GW begins to partially reflect downwards. This is based on the physical reasoning that the GW must evolve continuously in space and time.

For an upward propagating GW, $dm/dt = m\nu/H^2 < 0$ from Eq. (62), so that m becomes more negative in time, even after the wave dissipates and reflects. Therefore, within the assumptions inherent in our derivation, as an upward propagating GW dissipates, its vertical wavelength becomes increasingly smaller with time, as argued in Section 4a using the dispersion relation. The GW solution is not reversible in time at the reflection altitude (e.g., m does not change sign there) because the ray equations are nonlinear due to the change of the kinematic viscosity and thermal diffusivity with altitude.

For an infinitesimal change along this ray's path,

$$\begin{aligned}
d\delta &= \frac{\nu}{\omega_{Ir}H}dm + \frac{m}{\omega_{Ir}H}d\nu \\
&= \frac{\nu}{\omega_{Ir}H}dm + \frac{m}{\omega_{Ir}H}\frac{d\nu}{dz}\frac{dz}{dt}\frac{dt}{dm}dm \\
&= -\frac{m\omega_{Ir}^2(1+\delta)^3}{k_H^2N^2}dm.
\end{aligned} \tag{64}$$

Integrating Eq. (64) along the GW's path from z_1 to z , the exact solution for a GW propagating in an isothermal atmosphere with $\text{Pr} = 1$ is

$$(1+\delta)^2 \left[\frac{\omega_{Ir}^2}{k_H^2N^2}(m^2 - m_1^2) + \frac{1}{(1+\delta_1)^2} \right] = 1, \tag{65}$$

where δ_1 and m_1 are evaluated at $z = z_1$. Typically, z_1 is taken to be several scale heights below the reflecting altitude so that $\delta_1 \simeq 0$ and m_1 is the vertical wavelength of the wave before dissipative effects come into play. Because this solution tracks a GW before and throughout its dissipation, it represents a significant improvement over previous efforts by Pitteway and Hines [1963].

5. Special anelastic solutions when $\text{Pr} = 1$, $|m_1| \gg 1/2H$ and $|m_1| \gg |k_H|$

a. Reflection and dissipation altitudes

As a special example of the solutions derived in Section 4, we consider high-frequency GWs for which $m_1^2 \gg 1/4H^2$ and $m_1^2 \gg k_H^2$. We can solve Eq. (58) for m under these approximation to yield

$$m \simeq \frac{H\omega_{Ir}}{2\nu} \left[\sqrt{1 + \frac{4\nu m_1}{H\omega_{Ir}}} - 1 \right]. \quad (66)$$

For $\nu \rightarrow 0$, Eq. (66) reduces to $m \simeq m_1$. However, as ν increases, λ_z decreases for GWs with initially large vertical wavelengths. Since $m_1^2 \simeq k_H^2 N^2 / \omega_{Ir}^2$, Eq. (65) becomes

$$(1 + \delta)^2 \frac{m^2}{m_1^2} \simeq 1. \quad (67)$$

At the reflection altitude, combining Eqs. (63) and (67), we obtain

$$\delta \simeq -\frac{1}{2}. \quad (68)$$

Using Eq. (67), this implies that at the reflection altitude,

$$m = 2m_1, \quad (69)$$

or that the vertical wavelength is one-half what it is far below the reflection altitude where dissipation is unimportant. The vertical wavelength continues to decrease after the GW reflects, as discussed in Sec. 4a. Using Eqs. (68)-(69), the kinematic viscosity where the GW reflects is

$$\nu_{\text{refl}} \sim \frac{\omega_{Ir} H}{4|m_1|}, \quad (70)$$

which occurs at the approximate altitude

$$z_{\text{refl}} \sim z_1 + H \ln \left(\frac{\omega_{Ir} H}{4|m_1| \nu_1} \right). \quad (71)$$

The momentum flux and body force profiles calculated in Section 3c can be utilized here with $\psi = 2$ since, from Eq. (59), the inverse decay rate is $\omega_{Ii} \simeq -\nu m^2$. Using Eq. (54) and assuming that wave reflection occurs above this peak altitude, the kinematic viscosity where the momentum flux profile peaks is

$$\nu_{\text{diss}} \simeq \frac{\omega_{Ir}}{2H|m|^3}. \quad (72)$$

Interestingly, apart from a factor of 3/2 instead of 2, this condition is virtually identical to the ‘‘amplitude balance criterion’’ estimated via less formal means by Pitteway and Hines [1963]. Using Eq. (72), the dissipation altitude, which is the altitude where the momentum flux profile peaks, is

$$z_{\text{diss}} \simeq z_1 + H \ln \left(\frac{\omega_{Ir}}{2H|m|^3\nu_1} \right). \quad (73)$$

At z_{diss} , $\delta \simeq 1/(2m^2H^2)$. Therefore, if a GW’s vertical wavelength is smaller than $\sim \pi H$, then $\delta \simeq 0$ at the dissipation altitude, so that the GW’s vertical wavelength changes little during dissipation ($m_{\text{diss}} \simeq m_1$ from Eq. (67)). Note that GWs with the largest vertical wavelengths and highest frequencies dissipate at the highest altitudes. Thus atmospheric molecular viscosity and thermal diffusivity act as selective filters on upward-propagating GWs, removing smaller-scale, lower-frequency GWs at lower altitudes and larger-scale, higher-frequency GWs at higher altitudes [Hines, 1960].

b. Gravity wave dissipation and propagation characteristics

We can gain insight into the dissipative factors affecting a GW’s amplitude and dispersion by studying the Navier-Stokes horizontal and vertical momentum equations. Using Eqs. (13), (17), (18), (20) and (24), the horizontal momentum equation can be written

$$\tilde{u}_0(\omega_{Ii} - i\omega_{Ir}) = -ikR\tilde{T}_0 - \frac{ikc_s^2}{\gamma\rho_0}\tilde{\rho}_0 + \tilde{u}_0 \left\{ -\nu \left(\mathbf{k}^2 - \frac{1}{4H^2} \right) + \frac{im\nu}{H} \right\}. \quad (74)$$

The acceleration of the horizontal wind amplitude, apart from the exponential increase with altitude, is the real and imaginary terms on the LHS of Eq. (74). The real component, ω_{Ii} , is the GW amplitude decay from dissipation, while the imaginary component, $-i\omega_{Ir}$, is the rate of change of the oscillation. The dissipative terms are enclosed in curly brackets in Eq. (74), and are also comprised of real and imaginary components. The real component derives from ∇^2 operating on the oscillatory wave structure and the exponential amplitude increase with altitude, while the imaginary component comes from the cross terms. The real component is the explicit GW amplitude decrease from molecular viscosity, $\omega_{Ii} \simeq -\nu(\mathbf{k}^2 - 1/4H^2)$, although there are additional implicit contributions from the other terms on the RHS of Eq. (74) when $\text{Pr} \neq 1$ (compare Eqs. (25) and (59)). The imaginary component is the explicit change in GW frequency in time due to viscous dissipation, and is due entirely to the exponential wave amplitude increase with altitude.

This effect is significant for GWs with large vertical wavelengths. For GWs with small vertical wavelengths, the frequency change in time is insignificant even though the GW amplitudes decay from dissipation. The quantity, $\omega_{Ir} + m\nu/H = \omega_{Ir}(1 + \delta)$, can be thought of as a “generalized” GW intrinsic phase speed, since this quantity relates to the GW structure and background in a familiar way through the dispersion relation (compare Eqs. (1) and (58)). For $\text{Pr} \neq 1$, however, the generalization is more complicated (see Eq. (26)). Because δ becomes more negative as an upward propagating GW dissipates, this generalized intrinsic phase speed decreases in time, with the accompanying result that the GW vertical wavelength decreases in time.

We can understand GW propagation characteristics and the subsequent vertical wavelength decrease to some degree by examining the polarization relations. Using Eqs. (B.5), (B.4), (21), (24) and (59), the ratio of the GW horizontal to vertical amplitudes are

$$\frac{\tilde{u}_0}{\tilde{w}_0} \simeq -\frac{m}{k} \frac{(1 + \delta)}{(1 + (2 - 1/\gamma)\delta)}, \quad (75)$$

where we have assumed that $\text{Pr} = 1$, $m^2 \gg k_H^2$ and $m^2 \gg 1/4H^2$. Since $\delta \simeq 1/(2m^2H^2)$ at the dissipation altitude (using Eq.(73)), then at and below the dissipation altitude, Eq. (75) becomes

$$\frac{\tilde{u}_0}{\tilde{w}_0} \simeq -\frac{m}{k} \left(1 - \frac{(\gamma - 1)}{\gamma}\delta\right) \simeq -\frac{m}{k}. \quad (76)$$

Thus, at and below the dissipation altitude, Eq.(76) implies that the GW vertical wind amplitude decreases as compared to the GW horizontal wind amplitude when λ_z decreases. Thus, as a GW encounters exponentially increasing dissipation, parcel orbits flatten towards the horizontal in response, in agreement with the corresponding decrease in λ_z .

c. Characteristic times for gravity wave dissipation

The GW wind amplitudes are proportional to $\sqrt{\rho_0/\bar{\rho}} \exp(-i\omega_I t) \propto \exp(z/2H - t/\tau)$, where $\tau = -1/\omega_{Ii} \simeq 1/\nu m^2$ is the dissipative decay time at a given location using Eq. (59). Using Eq. (72) and $c_{gz} \simeq -\omega_{Ir}/m$, the decay time at the dissipation altitude is

$$\tau_{\text{diss}} \simeq \frac{4\pi}{\omega_{Ir}} \left(\frac{H}{|\lambda_z|} \right) \simeq \frac{2H}{c_{gz}}. \quad (77)$$

Thus, τ_{diss} is the time taken for a GW to propagate two density scale heights vertically. Because a GW's amplitude increases by $\exp(1)$ over two scale heights, these two effects cancel at z_{diss} . GWs with the largest vertical wavelengths and highest frequencies dissipate most quickly. We note that Eq. (77) does not hold for GWs with very large vertical wavelengths because of the ray-trace assumption inherent in deriving Eq. (77); these GWs are expected to dissipate at the dissipation altitude over a wave period or two.

d. Effective viscosity of $\nu(1 + \text{Pr}^{-1})$

As noted after Eq. (23), the combination of molecular viscosity and thermal diffusivity does not lead to a simple rescaling of the molecular viscosity from ν to $\nu(1 + \text{Pr}^{-1})$ mathematically. However, for high-frequency GWs with $\text{Pr} = 1$ and $m^2 \gg 1/4\text{H}^2$, it turns out that this simple scaling is a very good approximation at and below the dissipation altitude because $\alpha^2\nu^2/\text{Pr}$ is negligible. Using $\alpha^2 \simeq -m^2 + im/\text{H}$ and $\omega_I \simeq \omega_{Ir} - i\nu m^2$, the real part of the LHS of Eq. (23) when $\text{Pr} = 1$ is

$$\begin{aligned} \text{real}(\text{LHS}) &= \text{real}(\omega_I^2 - 2i\nu\alpha\omega_I - \{\alpha^2\nu^2\}) \\ &= \omega_{Ir}^2 + \nu^2 m^4 + \frac{2\nu\omega_{Ir}m}{\text{H}} + \left\{ -\nu^2 m^4 + \frac{\nu^2 m^2}{\text{H}^2} \right\}, \end{aligned} \quad (78)$$

where the contribution $\alpha^2\nu^2$ is contained in the curly brackets. Note that the appropriate terms cancel to yield the LHS of Eq. (58). Comparing the magnitude of the $\alpha^2\nu^2$ term with the other terms in Eq. (78), it is seen to be negligible when $|\nu^2 m^4| \ll |2\nu\omega_{Ir}m/\text{H}|$ or when

$$\nu \ll \frac{2\omega_{Ir}}{m^3\text{H}}. \quad (79)$$

Combining with Eq. (72), the condition that $\alpha^2\nu^2$ is negligible is that

$$\nu \ll 4\nu_{\text{diss}}. \quad (80)$$

Because the kinematic viscosity increases exponentially with height, this shows that $\alpha^2\nu^2$ is negligible at altitudes at and below the dissipation altitude. Therefore, the kinematic viscosity and thermal diffusivity add linearly as an effectively enhanced molecular viscosity of $\nu(1 + \text{Pr}^{-1})$ at and below the dissipation altitude where the GW momentum flux is most important.

6. Dissipation and reflection of high-frequency gravity waves

We now ray trace high-frequency GWs with differing vertical wavelengths numerically through isothermal atmospheres with differing Prandtl numbers. The initial wavelength pairs (λ_x, λ_z) are (100, 50), (40, 20), (20, 10), and (10, 5) km, where $\lambda_x \equiv 2\pi/|k|$. Fig. 1a-b show the GW ray paths until well beyond the times at which each wave dissipates (i.e., until $\overline{u'w'} \simeq 10^{-12}\overline{u'w'}_0$, where $\overline{u'w'}$ is the GW momentum flux per unit mass, and $\overline{u'w'}_0$ is its value at $z = z_0 = 0$), in order to ensure that the GW has fully dissipated by the end of ray-tracing. The boxes, diamonds, and triangles identify the dissipation altitudes, z_{diss} . As a GW propagates upwards, ν increases as the mean density decreases. However it is apparent from Fig. 1a that the ray paths are essentially unaffected by increasing ν until a few scale heights below z_{diss} , and only then for GWs with large λ_z . Although all of these GWs have identical frequencies of $\omega_{Ir} = N/\sqrt{5} = 0.45N$, because the vertical group velocities are $c_{gz} = -m\omega_{Ir}/\mathbf{k}^2 \simeq -\omega_{Ir}/m$, GWs with the largest λ_z (smallest m) propagate most quickly into the thermosphere. For example, the GWs with $\lambda_z = 50$ km arrive in the thermosphere shortly after 1 hour, while GWs with $\lambda_z = 5$ km arrive there after 6 – 7 hours. More importantly, those GWs with the largest λ_z dissipate at the highest altitudes, while those GWs with the smallest λ_z dissipate at the lowest altitudes. For example, for $\text{Pr} = 0.7$, the GWs with $\lambda_z = 50$ km and $\lambda_z = 5$ km have maximum momentum fluxes (per unit mass) at 152 and 112 km, respectively, which is a difference in altitude of almost 6 scale heights. This low dissipation altitude for the small λ_z GWs will yield much smaller momentum deposition than the large λ_z GWs (see Fig. 3), because the mean density at 112 km is larger than at 152 km by $\exp((152 - 112)/7) \simeq 300$. The higher dissipation altitudes obtained for GWs with large λ_z is a consequence of the steep proportionality of ν_{diss} with λ_z : $\nu_{\text{diss}} \propto \lambda_z^3$ (see Eq. (72)).

A large λ_z GW dissipates strongly within a scale height of where it reflects, as can be seen in detail in Fig. 1b. A small λ_z GW, however, dissipates at much lower altitudes, well before it reflects, as predicted in Secs. 3a and 5a. When only kinematic viscosity is included, GWs with $\lambda_z < 20$ km appear to “shoot” up to relatively high altitudes just below their reflecting altitude. However, this behavior is not physical and thus not relevant to GW forcing of the thermosphere.

Our derivations, solutions, and results are based on the validity of the WKB approxi-

mation. Einaudi and Hines (1970) showed that the WKB approximation is valid as long as the residue is much less than one, where the residue is defined in our notation as (Eq. (4) and (59) of Einaudi and Hines, 1970)

$$R_2 = \frac{1}{2m^3} \frac{d^2m}{dz^2} - \frac{3}{4m^4} \left(\frac{dm}{dz} \right)^2. \quad (81)$$

When the residue is of order one or larger, the WKB approximation fails because the solution cannot be written as only an upgoing or only a downgoing GW. For example, if an upgoing GW encounters significant dissipation and suffers significant (partial) reflection above a certain altitude, then the calculated residue will be larger than one above that altitude, because the solution is given by a superposition of upgoing and downgoing GWs with altitude dependence, rather than just by an upgoing wave. We will not construct such a solution here. Instead, we identify the range of altitudes and times where a GW has $R_2 \geq 1$.

In Fig. 1b, the regions between the small, dark circles show the locations along the ray paths where the residue is larger than one ($R_2 \geq 1$). For some of the rays, this occurs over a very short period of time and altitude range (e.g., those rays propagating through an atmosphere with molecular viscosity only), while for other rays, this altitude range is somewhat larger. Notice that the solution after reflection and below the dark circles are valid WKB solutions.

Fig. 2a shows the evolution of $2\pi/m$ for GWs from Fig. 1 as a function of time. As predicted in Sec. 4b, GW λ_z decrease near and especially beyond z_{diss} for $\text{Pr} = 1$. Large initial λ_z have already decreased at z_{diss} while small initial λ_z do not decrease until after their momentum fluxes become negligible. Once λ_z begins to decrease, it decreases rapidly in time. For GWs with $\lambda_z = 10$ km, the unusual behavior noted above for $\text{Pr} = \infty$ can be clearly seen; λ_z first increases then decreases. This is severely accentuated for the GW with initial $\lambda_z = 5$ km.

Fig. 2b shows the evolution with altitude of the GWs with the largest λ_z . As before, the regions between the small, dark circles show the locations along the ray paths where the residue is greater than one. For all GWs, λ_z decreases ($|m|$ increases) significantly during wave dissipation and prior to reaching altitudes at which $R_2 \geq 1$. While λ_z decreases during dissipation for all Pr , the altitude at which this occurs varies. Here, λ_z

begins to decrease approximately two scale heights below where the momentum fluxes are maximum. For all Pr, λ_z decreases by a factor of ~ 2 by the time each GW reaches z_{refl} (see Eq. (69)).

Fig. 2c displays the comparison between the numerical solutions and the exact and approximate Pr = 1 solutions given by Eqs. (65) and (67), respectively, for the GWs with the largest λ_z . These solutions explore the region where λ_z changes rapidly, which occurs within a few scale heights of z_{diss} . The exact Pr = 1 solution, Eq. (65), is satisfied virtually exactly, as expected, when the wave propagates through a Pr = 1 atmosphere. For Pr = 0.7, Eq. (65) provides a good approximation of the solution until the wave dissipates; thereafter, the solution diverges. For Pr = ∞ (i.e., kinematic viscosity only), Eq. (65) does not approximate the exact solution very well because the GW dissipates approximately a scale height higher than for Pr = 1. Note that the approximate solution, Eq. (67), is only marginally satisfied for Pr = 1 because the assumption inherent in this approximation (i.e., that $m^2 \gg k_H^2 + 1/4H^2$) is not well satisfied. GWs at lower frequencies agree more closely with this approximate solution (not shown). However, low-frequency waves are not relevant for the forcing of the lower thermosphere (Vadas and Fritts, 2004), since only those waves with the highest frequencies (above any intervening shears) propagate to and dissipate at the highest altitudes.

Altitude profiles of binned momentum fluxes for the GWs discussed above are shown in Fig. 3, labeled by initial λ_z . The scaling factor decreases from left to right by an order of magnitude for each panel. The momentum fluxes are largest for the GWs with the largest λ_z . For example, for Pr = 0.7 the maximum momentum flux for the GW with initial $\lambda_z = 50$ km is ~ 8 times larger than for the GW with initial $\lambda_z = 20$ km, and the latter value is ~ 7 times larger than for the GW with initial $\lambda_z = 10$ km. Note that the GWs have dissipated substantially by the time they reach the altitude of peak momentum flux, and that the GW momentum fluxes decrease rapidly with altitude above the dissipation altitude. The residues are greater than one for the altitudes above the small, dark circles. Note that the GW momentum fluxes are small or negligible where $R_2 \geq 1$ because of dissipation.

For given initial parameters, GWs propagating through an atmosphere with kinematic viscosity only (Pr = ∞) dissipate and reflect at higher altitudes than those experiencing

finite Pr. For example, the GW with initial $\lambda_z = 50$ (20) km yields maximum momentum fluxes at $\simeq 152$, 153 and 158 km (139, 141 and 146 km) for Pr = 0.7, 1, and ∞ , respectively. Thus kinematic viscosity only, results in momentum deposition approximately a scale height above that for an atmosphere with Pr = 0.7. Thus, we expect the lower thermospheric body forcing results of Vadas and Fritts (2004) to be lowered in altitude by $\sim H$ in accounting for both kinematic viscosity and thermal diffusivity. Note that the dissipation altitude is 1-2 km higher for Pr = 1 than for Pr = 0.7 when $H = 7$ km.

The first four columns of Table 1 show the calculated vertical wavelengths and dissipation times at z_{diss} for the Pr = 1 ray-traced GWs. The calculated dissipation time, Δt_{diss} , is chosen to be the time along the ray's path from when the zonal velocity is maximum to when the zonal velocity is e^{-1} times the maximum. The last two columns of the table display the estimated dissipation altitudes (using Eq. (73)), as well as the the estimated decay times at the dissipation altitudes, τ_{diss} , using Eq. (77). For these calculations, we set $m = 2\pi/\lambda_{\text{diss}}$, where λ_{diss} is the vertical wavelength at the dissipation altitude. These formulas approximate the dissipation altitudes and times very well, with discrepancies arising from the assumption that $m^2 \gg k_H^2$ (which is only approximately satisfied in this example). GWs with small vertical wavelengths dissipate much more slowly and at much lower altitudes than those with large vertical wavelengths.

Body force profiles arising from the dissipation of the GWs with initial $\lambda_z = 50$ and 10 km and Pr = 1 discussed above are shown in Fig. 4 using Eq. (50). As with the momentum fluxes, the body forces are largest for the GWs having the largest λ_z . The GW with initial $\lambda_z = 50$ km (solid) creates a body force at $z \simeq 156$ km with a maximum acceleration of $1 \times 10^6 \text{ m}^{-1} \times \overline{u'w'_0}$, while the GW with initial $\lambda_z = 10$ km (dash-dot) creates a body force at a much lower altitude of 133 km with a much smaller maximum acceleration of $7 \times 10^3 \text{ m}^{-1} \times \overline{u'w'_0}$. The body force for the deeper GW is much more confined spatially. This occurs because λ_z for the initially deeper wave shortens considerably accompanying dissipation, thereby decreasing the GW amplitude more quickly in altitude (see Eq. (51)). Also shown in Fig. 4 are profiles obtained from Eq. (53) using these same parameters. The fit is excellent for the GW with initially small λ_z because the approximation that the GW λ_z does not change during dissipation is satisfied. However, Eq. (53) does not yield a good approximation for the body force for

the GW with initially larger λ_z , because λ_z shortens substantially during GW dissipation (thus invalidating the assumption that went into deriving Eq. (53)).

7. Increasing thermospheric temperatures

Although the lower and middle atmospheres vary relatively little from $\bar{T} \simeq 250$ K (except near the summer polar mesosphere), temperature increases rapidly above ~ 100 km. An extreme minimum thermospheric temperature is $\bar{T} \sim 550$ K under solar minimum conditions, implying a density scale height of $H \geq 15$ km. A larger density scale height at higher altitudes implies that at a given altitude, the kinematic viscosity, $\nu = \mu/\bar{\rho}$, is smaller than it would be in a purely isothermal atmosphere. A smaller kinematic viscosity implies that a GW can propagate higher in altitude before dissipating, since the dissipation altitude depends only on the local kinematic viscosity and is approximately proportional to the scale height (see Eqs. (72)-(73)). If the scale height doubles above an altitude of z_d , for example, the distance a GW propagates above z_d before dissipating doubles as compared to the distance when $\bar{T} = 250$ K above that altitude. Therefore, the dissipation altitudes determined in Secs. 4-6 (assuming $\bar{T} = 250$ K and $H = 7$ km) are much lower than would occur in an atmosphere with a more realistic thermal structure.

Vadas and Fritts (2004) ray-traced a modeled spectrum of GWs from mesoscale convective complexes (MCCs) through an isothermal atmosphere with molecular viscosity only and found that the GWs led to maximum body forcings at ~ 165 km. In order to estimate the actual altitude, they calculated the altitude where the kinematic viscosity for a more realistic temperature profile is the same as the kinematic viscosity in an isothermal atmosphere. Using this estimate, they found that $z \simeq 165$ km in the isothermal atmosphere has an equivalent kinematic viscosity at $z \sim 200$ km in an extreme minimum temperature thermosphere. This led them to estimate that GWs from MCCs would create body forcings at $z \sim 200$ km under extreme solar minimum conditions, and higher for larger thermospheric temperatures, giving credence to the possibility that GW dissipation in the lower thermosphere may seed equatorial spread-F (ESF) bubbles. Note that because the GW momentum fluxes grow with altitude as the inverse density, the higher altitudes attained with larger thermospheric temperatures result in the same momentum deposition at dissipation altitudes.

On the other hand, GW amplitudes and momentum fluxes arising from MCCs will be largest at a specific altitude at extreme minimum thermospheric temperatures because lower temperatures imply smaller H and more rapid amplitude growth above ~ 100 km (apart from dissipation). The prediction of larger GW amplitudes near 200 km at solar minimum appears to correlate with stronger ESF and plasma bubble activity observed under these conditions (Hysell and Burcham, 2002). The larger dissipation under solar minimum conditions may itself be linked to the occurrence of initial ESF at lower altitudes, though this may be due instead (or in addition) to a lower bottomside F layer under these conditions.

8. Summary and Conclusions

In this paper, we derived a 3D, anelastic gravity wave (GW) dispersion relation for internal, high-frequency GWs that takes into account the effects of both kinematic viscosity and thermal diffusivity, both of which are important at GW scales in the thermosphere. We also derived the decay rate of the GW amplitude in time. This dispersion relation is an improvement over past efforts because it can be utilized before, during, and after a GW dissipates, not just when dissipation is a small effect. This is essential for the understanding of thermospheric accelerations created by diverse, localized, and intermittent GW sources. In the limit that dissipation is negligible, the usual GW anelastic dispersion relation is obtained. Considered individually, molecular viscosity has the same effect on a GW's dissipation as thermal diffusivity. Molecular viscosity and thermal diffusivity together, however, cannot be characterized simply as an enhanced viscosity in general. However, for GWs with $m^2 \gg 1/4H^2$ and for a Prandtl number (Pr) of one, the effects add together linearly at and below the dissipation altitude.

In the special case that the thermal structure is isothermal, the winds are constant near the dissipation altitude, and $\text{Pr} = 1$, a simple GW dispersion relation and amplitude decay rate are obtained. This relation and decay rate yield significant insights, including at what altitude a GW dissipates, how this dissipation altitude depends on and affects a GWs intrinsic parameters (such as vertical wavelength and frequency), and how this dissipation altitude depends on slowly-varying background parameters (such as temperature and density scale height). It is found that the effect of dissipation on a GW is

similar to the effect of shear in the sense that as the kinematic viscosity and thermal diffusivity increase due to decreasing background density, the generalized intrinsic frequency (i.e., the intrinsic frequency plus $m\nu/H$) decreases, causing λ_z to decrease. At the same time, the GW parcel orbits flatten towards the horizontal and the GW propagates more horizontally. Thus, unlike the Boussinesq case with kinematic viscosity only, the vertical wavelength of a large λ_z GW decreases in a $\text{Pr} = 1$ atmosphere as dissipation increases. It can also be shown that for high-frequency, upward-propagating GWs with $\omega_{Ir}/N < 1$ and $\mathbf{k}^2 \simeq m^2$, a GW dissipates when $\nu_{\text{diss}} \simeq \omega_{Ir}/2H|m|^3$ or at the altitude $z_{\text{diss}} \simeq z_1 + H \ln(\omega_{Ir}/2H|m|^3\nu_1)$. This implies that GW dissipation does not depend on an integrated viscosity effect, but rather on the local value of viscosity. Therefore, in a more realistic environment where the temperature increases rapidly above 100 km, the scale height also increases rapidly, causing the viscosity to increase less rapidly with altitude as compared to an isothermal atmosphere. This will cause a GW to propagate to much higher altitudes before reaching the same value of ν which causes its rapid dissipation. This analytic solution also provides the insight that GWs with high frequencies and large vertical wavelengths will propagate to the highest altitudes. Because GW momentum fluxes (per unit density) grow exponentially with altitude prior to dissipation, those GWs dissipating at the highest altitudes will have a much larger effect on the thermosphere than those dissipating at lower altitudes. Molecular viscosity and thermal diffusivity, therefore, act as selective filters on a GW spectrum, allowing only those high-frequency, large vertical wavelength GWs to propagate to the highest altitudes.

Using our 3D ray trace code, we verified that high-frequency GWs with large λ_z dissipate at the highest altitudes. For example, for high-frequency GWs with $\omega/N \simeq 0.45$, dissipation altitudes in an isothermal, $\text{Pr} = 1$ atmosphere are 155, 140, 130, and 115 km for GWs with initial $\lambda_z = 50, 20, 10$ and 5 km, respectively. We also verified that our analytic results estimate these calculated altitudes well, and that during dissipation, λ_z decreases for GWs with initially large λ_z . The vertical wavelengths of GWs with initially small λ_z , however, do not change during dissipation.

We also used our 3D ray trace code to determine what effect the Prandtl number has on thermospheric penetration. We found that high-frequency GWs with large λ_z dissipate approximately a scale height lower for $\text{Pr} = 0.7$ than for $\text{Pr} = \infty$. We also found that

the dissipation altitudes are only a km or two higher for $\text{Pr} = 1$ than for $\text{Pr} = 0.7$. For $\text{Pr} = 1$ and $\text{Pr} = \infty$, we derived analytic formulae for the GW momentum fluxes and resulting body forces under certain approximations. We find that the maximum body forces occur $\sim 0.7H$ above the GW dissipation altitudes. These approximations are well satisfied for GWs with small λ_z because λ_z changes little during dissipation. However, results of numerical ray-tracing showed that these approximations work less well for GWs with large λ_z because λ_z changes rapidly during dissipation, resulting in a much narrower body force profile in altitude.

Finally, we discussed the ramifications of larger (more realistic) thermospheric temperatures. A previous effort (Vadas and Fritts, 2004) estimated body force altitudes from GWs from MCCs to be ~ 200 km accompanying minimum temperature thermospheres for dissipation due only to kinematic viscosity. Our current, more complete analysis allows us to estimate that GWs from MCCs create thermospheric body forcings $\sim H$ lower, or at ~ 185 km accompanying minimum thermospheric temperatures for $\text{Pr} = 0.7$. Further quantification of GW penetration into the thermosphere, however, will require numerical ray-tracing in realistic mean temperatures (and winds) under solar minimum and solar maximum conditions (Vadas and Fritts, work in progress).

Acknowledgments This research was supported by the National Aeronautics and Space Administration under contract NAS5-02036, the National Science Foundation under grant ATM-0307910, and the Air Force Office of Scientific Research under contract F49620-00-C-0045. We gratefully acknowledge the helpful comments from an anonymous reviewer, M.P. Hickey, and C.O. Hines.

Appendix A: Neglecting the second molecular viscosity term

It is easy to show that $|\nabla^2 \mathbf{v}'| \gg |(1/3) \nabla(\nabla \cdot \mathbf{v}')|$ using the expressions for \mathbf{v}' with molecular viscosity only, provided $\lambda_z \ll 4\pi H$. Eq. (B.5) is the anelastic polarization relation for the horizontal velocity in the presence of molecular viscosity. Setting $\text{Pr} = \infty$ and assuming $m^2 \gg 1/4H^2$, this relation becomes

$$\tilde{u}_0 \simeq -\frac{m}{k} \left[1 + \frac{i}{mH} \left(\frac{1}{\gamma} - \frac{1}{2} \right) \right] \tilde{w}_0. \quad (\text{A.1})$$

Using

$$\frac{\partial}{\partial x}(\nabla \cdot \mathbf{v}') = \sqrt{\frac{\rho_0}{\bar{\rho}}} \left[\tilde{u}_{xx} + \tilde{w}_{xz} + \frac{1}{2H} \tilde{w}_x \right] \quad (\text{A.2})$$

$$\frac{\partial}{\partial z}(\nabla \cdot \mathbf{v}') = \sqrt{\frac{\rho_0}{\bar{\rho}}} \left[\tilde{u}_{xz} + \tilde{w}_{zz} + \frac{1}{H} \tilde{w}_z + \frac{1}{2H} \tilde{u}_x + \frac{1}{4H^2} \tilde{w} \right] \quad (\text{A.3})$$

$$\nabla^2 u' = \sqrt{\frac{\rho_0}{\bar{\rho}}} \left[\tilde{u}_{xx} + \tilde{u}_{zz} + \frac{1}{H} \tilde{u}_z + \frac{1}{4H^2} \tilde{u} \right] \quad (\text{A.4})$$

$$\nabla^2 w' = \sqrt{\frac{\rho_0}{\bar{\rho}}} \left[\tilde{w}_{xx} + \tilde{w}_{zz} + \frac{1}{H} \tilde{w}_z + \frac{1}{4H^2} \tilde{w} \right], \quad (\text{A.5})$$

and Eq. (18) for u' and w' , the ratio of the viscous terms for the x -component is

$$\frac{\frac{\partial}{\partial x}(\nabla \cdot \mathbf{v}')}{\nabla^2 u'} \simeq \frac{ik^2}{\gamma H m} \left[\frac{1}{k^2 + m^2} + \frac{i}{mH(k^2 + m^2)^2} \left(m^2 - (k^2 + m^2) \left(\frac{1}{\gamma} - \frac{1}{2} \right) \right) \right]. \quad (\text{A.6})$$

Regardless of the magnitudes of k and m , the absolute magnitude of Eq. (A.6) is much less than one. The ratio of the viscous terms for the z -component is

$$\begin{aligned} \frac{\frac{\partial}{\partial z}(\nabla \cdot \mathbf{v}')}{\nabla^2 w'} \simeq & -\frac{1}{(1 + k^2/m^2)^2} \left[\frac{i}{\gamma H m} \left(1 + \frac{k^2}{m^2} \right) - \frac{1}{\gamma H^2 m^2} \right. \\ & \left. + \frac{1}{2H^2 m^2} \left(\frac{1}{\gamma} - \frac{1}{2} \right) \left(1 + \frac{k^2}{m^2} \right) + \frac{i}{2H^3 m^3} \left(\frac{1}{\gamma} - \frac{1}{2} \right) \right]. \end{aligned} \quad (\text{A.7})$$

Again, regardless of the magnitudes of k and m , the absolute magnitude of Eq. (A.7) is much less than one. Therefore, we have shown that $(1/3) \nabla(\nabla \cdot \mathbf{v}')$ can be neglected with respect to $\nabla^2 \mathbf{v}'$ when molecular viscosity is included, provided that the GW has $\lambda_z \ll 4\pi H$. Because we showed in Sec. 5d that molecular viscosity and thermal diffusivity add linearly up to the dissipation altitude for $\text{Pr} = 1$, we therefore conclude that $|(1/3) \nabla(\nabla \cdot \mathbf{v}')| \ll |\nabla^2 \mathbf{v}'|$ under the same circumstances.

Appendix B: Polarization relations

The compressible GW polarization relations accompanying the compressible dispersion relation given by Eq. (19) are

$$\tilde{u}_0 = \frac{1}{ikc_s^2 \mathcal{D}} \left[\gamma i \omega_I (i \omega_I + \alpha \nu) \left(i \omega_I + \frac{\gamma \alpha \nu}{\text{Pr}} \right) + \gamma c_s^2 \left(m^2 + \frac{1}{4H^2} \right) \left(i \omega_I + \frac{\alpha \nu}{\text{Pr}} \right) \right] \tilde{w}_0 \quad (\text{B.1})$$

$$\tilde{T}_0 = \frac{(\gamma - 1) \bar{T}}{c_s^2 \mathcal{D}} \left[\gamma i \omega_I (i \omega_I + \alpha \nu) + \frac{c_s^2}{H} \left(im + \frac{1}{2H} \right) \right] \tilde{w}_0 \quad (\text{B.2})$$

$$\tilde{\rho}_0 = \frac{\rho_0}{i\omega_I c_s^2 \mathcal{D}} \left[\gamma i\omega_I (i\omega_I + \alpha\nu) \left(i\omega_I + \frac{\gamma\alpha\nu}{\text{Pr}} \right) - \frac{i(\gamma-1)\omega_I c_s^2}{\text{H}} \left(im - \frac{1}{2\text{H}} \right) \right] \tilde{w}_0, \quad (\text{B.3})$$

where the denominator is

$$\mathcal{D} = \left[i\omega_I \left(\gamma im + \frac{1}{\text{H}} - \frac{\gamma}{2\text{H}} \right) + \frac{\gamma\alpha\nu}{\text{Pr}} \left(im + \frac{1}{2\text{H}} \right) \right]. \quad (\text{B.4})$$

The expression for \tilde{v}_0 can be obtained trivially by replacing $k \rightarrow l$ in Eq. (B.1). Neglecting terms of order $(\omega_I/c_s)^2$, the anelastic, GW, polarization relations are

$$\tilde{u}_0 \simeq \frac{\gamma}{ik\mathcal{D}} \left(m^2 + \frac{1}{4\text{H}^2} \right) \left(i\omega_I + \frac{\alpha\nu}{\text{Pr}} \right) \tilde{w}_0 \quad (\text{B.5})$$

$$\tilde{T}_0 \simeq \frac{(\gamma-1)\bar{T}}{\text{H}\mathcal{D}} \left(im + \frac{1}{2\text{H}} \right) \tilde{w}_0 \quad (\text{B.6})$$

$$\tilde{\rho}_0 \simeq -\frac{(\gamma-1)\rho_0}{\text{H}\mathcal{D}} \left(im - \frac{1}{2\text{H}} \right) \tilde{w}_0. \quad (\text{B.7})$$

Appendix C: Derivatives needed for ray-tracing

Taking the partial derivative of Eq. (26) with respect to k , l , m , and x_i (where x_i is x , y , or z), and solving for $\partial\omega_{Ir}/\partial k$, etc., we obtain:

$$c_{g_x} = \frac{k}{\omega_{Ir}\mathcal{B}} \left[\frac{N^2(m^2 + 1/4\text{H}^2)}{(\mathbf{k}^2 + 1/4\text{H}^2)^2} - \frac{\nu^2}{2}(1 - \text{Pr}^{-1})^2 \left(\mathbf{k}^2 - \frac{1}{4\text{H}^2} \right) \frac{(1 + \delta_+ + \delta^2/\text{Pr})}{(1 + \delta_+/2)^2} \right] \quad (\text{C.1})$$

$$c_{g_y} = \frac{l}{\omega_{Ir}\mathcal{B}} \left[\frac{N^2(m^2 + 1/4\text{H}^2)}{(\mathbf{k}^2 + 1/4\text{H}^2)^2} - \frac{\nu^2}{2}(1 - \text{Pr}^{-1})^2 \left(\mathbf{k}^2 - \frac{1}{4\text{H}^2} \right) \frac{(1 + \delta_+ + \delta^2/\text{Pr})}{(1 + \delta_+/2)^2} \right] \quad (\text{C.2})$$

$$c_{g_z} = \frac{1}{\omega_{Ir}\mathcal{B}} \left\{ m \left[-\frac{k_H^2 N^2}{(\mathbf{k}^2 + 1/4\text{H}^2)^2} - \frac{\nu^2}{2}(1 - \text{Pr}^{-1})^2 \left(\mathbf{k}^2 - \frac{1}{4\text{H}^2} \right) \frac{(1 + \delta_+ + \delta^2/\text{Pr})}{(1 + \delta_+/2)^2} \right. \right. \\ \left. \left. + \frac{\nu^4(1 - \text{Pr}^{-1})^4 (\mathbf{k}^2 - 1/4\text{H}^2)^2}{16\text{H}^2\omega_{Ir}^2} \frac{1}{(1 + \delta_+/2)^3} - \frac{\nu^2}{\text{Pr H}^2} \right] - \frac{\nu_+ \omega_{Ir}}{2\text{H}} \right\} \quad (\text{C.3})$$

$$\begin{aligned}
\frac{\partial \omega_{Ir}}{\partial x_i} = & \frac{1}{\omega_{Ir} \mathcal{B}} \left\{ \frac{k_H^2 N}{(\mathbf{k}^2 + 1/4H^2)} \frac{\partial N}{\partial x_i} \right. \\
& + \left[\frac{k_H^2 N^2}{4(\mathbf{k}^2 + 1/4H^2)^2} - \frac{\nu^2}{8} (1 - \text{Pr}^{-1})^2 \left(\mathbf{k}^2 - \frac{1}{4H^2} \right) \frac{(1 + \delta_+ + \delta^2/\text{Pr})}{(1 + \delta_+/2)^2} \right. \\
& \left. - \frac{\delta^2 \nu^2 H^2 (1 - \text{Pr}^{-1})^4 (\mathbf{k}^2 - 1/4H^2)^2}{16 (1 + \delta_+/2)^3} + \frac{\nu_+ m \omega_{Ir} H}{2} + \frac{\nu^2 m^2}{\text{Pr}} \right] \left(H^{-3} \frac{\partial H}{\partial x_i} \right) \\
& + \left[-\frac{\nu (1 - \text{Pr}^{-1})^2 (\mathbf{k}^2 - 1/4H^2)^2}{16 (1 + \delta_+/2)^3} \left(4 + 6\delta_+ + \left(1 + \frac{10}{\text{Pr}} + \frac{1}{\text{Pr}^2} \right) \delta^2 \right. \right. \\
& \left. \left. + \frac{2(1 + \text{Pr}^{-1})}{\text{Pr}} \delta^3 \right) - \frac{m \omega_{Ir} (1 + \text{Pr}^{-1})}{2H} - \frac{\nu m^2}{\text{Pr} H^2} \right] \frac{\partial \nu}{\partial x_i} \left. \right\} \quad (\text{C.4})
\end{aligned}$$

where the denominator is

$$\mathcal{B} = \left[1 + \frac{\delta_+}{2} + \frac{\delta^2 \nu^2}{16 \omega_{Ir}^2} (1 - \text{Pr}^{-1})^4 \frac{(\mathbf{k}^2 - 1/4H^2)^2}{(1 + \delta_+/2)^3} \right] \quad (\text{C.5})$$

These are the exact formulas needed for ray-tracing GWs using Eqs. (27)-(28), subject to the assumptions leading to their derivation.

References

- Del Genio, A.D. and G. Schubert, 1979: Gravity wave propagation in a diffusively separated atmosphere with height-dependent collision frequencies, *J. Geophys. Res.*, **84**, 4371–4378.
- Einaudi, F. and Hines, C.O. 1970: WKB approximation in application to acoustic-gravity waves, *Can. J. Phys.*, **48**, 1458–1471.
- Fritts, D. C., and M. J. Alexander, 2003: Gravity wave dynamics and effects in the middle atmosphere, *Rev. Geophys.*, **41**, 10.1029/2001RG000106.
- Gossard, E.E. and Hooke, W.H., 1975: Waves in the atmosphere, Elsevier Scientific Publishing Co., Amsterdam, 456 pp.
- Harris, K. K., Sharp, G. W. and Knudsen, W. C., 1969: Gravity waves observed by ionospheric temperature measurements in the F region, *J. Geophys. Res.*, **74**, 197–204.
- Hines, C.O. 1960: Internal atmospheric gravity waves at ionospheric heights, *Can. J. Phys.*, **38**, 1441–1481.
- Hines, C.O. 1967: On the nature of travelling ionospheric disturbances launched by low-altitude nuclear explosions, *J. Geophys. Res.*, **72**, 1877–1882.
- Hines, C.O. 1968a: An effect of molecular dissipation in upper atmospheric gravity waves, *J. Atmos. Solar Terres. Phys.*, **30**, 845–849.
- Hines, C.O. 1968b: An effect of ohmic losses in upper atmospheric gravity waves, *J. Atmos. Solar Terres. Phys.*, **30**, 851–856.
- Hines, C.O. 1973: A critique of multilayer analyses in application to the propagation of acoustic-gravity waves, *J. Geophys. Res.*, **78**, 265–273.
- Hocke, K., and K. Schlegel, 1996: A review of atmospheric gravity waves and traveling ionospheric disturbances: 1982 - 1995, *Ann. Geophys.*, **14**, 917–940.
- Huang, C. S., M. C. Kelley, and D. L. Hysell, 1993: Nonlinear Rayleigh-Taylor instabilities, atmospheric gravity waves, and equatorial spread-F, *J. Geophys. Res.*, **98**, 15,631.
- Huang, C. S., and M. C. Kelley, 1996a: Nonlinear evolution of equatorial spread-F. 1. On the role of plasma instabilities and spatial resonance associated with gravity wave seeding, *J. Geophys. Res.*, **101**, 283.

- Huang, C. S., and M. C. Kelley, 1996b: Nonlinear evolution of equatorial spread-F. 2. Gravity wave seeding of Rayleigh-Taylor instability, *J. Geophys. Res.*, **101**, 293.
- Huang, C. S., and M. C. Kelley, 1996c: Nonlinear evolution of equatorial spread-F. 4. Gravity waves, velocity shear, and day-to-day variability, *J. Geophys. Res.*, **101**, 24,523.
- Hysell, D. L., and J. D. Burcham, 2002: Long term studies of equatorial spread F using the JULIA radar at Jicamarca, *J. Atmos. Solar Terres. Phys.*, **64**, 1531–1543.
- Hysell, D. L., M. C. Kelley, W. E. Swartz, and R. F. Woodman, 1990: Seeding and layering of equatorial spread-F, *J. Geophys. Res.*, **95**, 17,253.
- Kundu, P., 1990: Fluid Dynamics, Academic Press, San Diego, 638 pp.
- Lighthill, J., 1978: Waves in Fluids, Cambridge University Press, Cambridge, 504 pp.
- Marks, C. J., and S. D. Eckermann, 1995: A three-dimensional nonhydrostatic ray-tracing model for gravity waves: Formulation and preliminary results for the middle atmosphere, *J. Atmos. Sci.*, **52**, 1959–1984.
- Midgley, J. E. and Liemohn, H. B., 1966: Gravity waves in a realistic atmosphere, *J. Geophys. Res.*, **71**, 3729–3748.
- Myers, R.M. and Yanowitch, M., 1971: Small oscillations of a viscous isothermal atmosphere, *J. Comp. Phys.*, **8**, 241–257.
- Newton, G. P., Pelz, D. T., and Volland, H., 1969: Direct in situ measurements of wave propagation in the neutral thermosphere, *J. Geophys. Res.*, **74**, 183–196.
- Oliver, W. L., Y. Otsuka, M. Sato, T. Takami, and S. Fukao, 1997: A Climatology of F Region Gravity Wave Propagation over the Middle and Upper Atmosphere Radar, *J. Geophys. Res.*, **102**, 14,499–14,512.
- Pitteway, M.L.V. and Hines, C.O., 1963: The viscous damping of atmospheric gravity waves? *Can. J. Phys.* '41'1935–1948.
- Press, W. H., S. A. Teukolsky, W. T. Vetterling, and B. P. Flannery, 1992: Numerical recipes in Fortran, Second Ed., Cambridge University Press, Cambridge, 963 pp.
- Sekar, R., R. Suhasini, and R. Raghavarao, 1995: Evolution of plasma bubbles in the equatorial F region with different seeding conditions, *Geophys. Res. Lett.*, **22**, 885.
- Sekar, R., and M. C. Kelley, 1998: On the combined effects of vertical shear and zonal electric field patterns on nonlinear equatorial spread F evolution, *J. Geophys. Res.*,

103, 20,735–20,747.

Thome, G. D., 1964: Incoherent scatter observations of traveling ionospheric disturbances, *J. Geophys. Res.*, **69**, 4047–4049.

Vadas, S. L, and D. C. Fritts, 2004: Thermospheric responses to gravity waves arising from mesoscale convective complexes, *J. Atmos. Solar Terres. Phys.*, **66**, 781–804.

Volland, H., 1969: Full wave calculations of gravity wave propagation through the thermosphere, *J. Geophys. Res.*, **74**, 1786–1795.

Yanowitch, M., 1967: Effect of viscosity on vertical oscillations of an isothermal atmosphere, *Can. J. Phys.*, **45**, 2003–2008.

Yanowitch, M., 1969: A Numerical study of vertically propagating waves in a viscous isothermal atmosphere, *J. Comp. Phys.*, **4**, 531–542.

Figure Captions

Figure 1. a): The ray paths for four high-frequency GWs which are initially located at $z = 0$ at $t = 0$. The solid, dash, and dash-dot lines are for GWs propagating through an isothermal atmosphere with $\text{Pr} = 0.7$, $\text{Pr} = 1.0$, and $\text{Pr} = \infty$, respectively. These GWs have $l = 0$ and are initially propagating upwards in a zero wind environment. Ray paths for the different wavelengths (see text) are labeled by initial vertical wavelengths (in km). The boxes, diamonds, and triangles show the altitudes and times at which the GW momentum fluxes (per unit density) are maximum for $\text{Pr} = 0.7$, $\text{Pr} = 1.0$, and $\text{Pr} = \infty$, respectively. b): An enlarged portion of a). The ray paths between the small dark circles have $R_2 \geq 1$ using Eq. (81).

Figure 2. a): $2\pi/m$ as a function of time for the GW ray paths displayed in Fig. 1. b): Vertical wavelength as a function of altitude for the initial $\lambda_z = 50$ km GWs shown in a). The vertical wavelengths between the small dark circles have $R_2 \geq 1$. c): Plots of the LHS of Eq. (65) (solid lines) and Eq. (67) (dot lines) for the GWs shown in b), labeled by Pr . In each panel, the symbols show where the GW momentum fluxes are maximum with the same meaning as in Fig. 1.

Figure 3. Altitude profiles in 0.1 km bins of GW momentum fluxes for the GW ray paths displayed in Fig. 1. Initial vertical wavelengths from left to right are 50, 20, 10, and 5 km. The scaling factors decrease from left to right by an order of magnitude in each panel. Dotted lines show the exponential increase in fluxes in the absence of dissipation. The momentum fluxes above the small dark circles have $R_2 \geq 1$.

Figure 4. Altitude profiles of created body forces for the GWs with initial $\lambda_z = 50$ km (solid line) and $\lambda_z = 10$ km (dash-dot line) propagating through an isothermal atmosphere with $\text{Pr} = 1$. Also shown are plots of Eq. (53) for these GWs (dash line and dash-dot-dot-dot line, respectively), with m evaluated at $z_0 = 0$. In order to fit both GW profiles in the same plot, the solid and dash lines are scaled by 10^{-6} , while the dash-dot and dash-dot-dot-dot lines are scaled by 10^{-4} .

Table 1: Gravity wave dissipation ($\text{Pr} = 1$)

$ \lambda_z(z_0) $	$ \lambda_z(z_{\text{diss}}) $	z_{diss} (km)	Δt_{diss}	z_{diss} (Eq. (73))	τ_{diss} (Eq. (77))
50 km	38 km	153 km	6 min	159 km	5 min
20 km	19 km	141 km	10 min	144 km	9 min
10 km	10 km	128 km	18 min	131 km	17 min
5 km	5 km	114 km	35 min	117 km	33 min

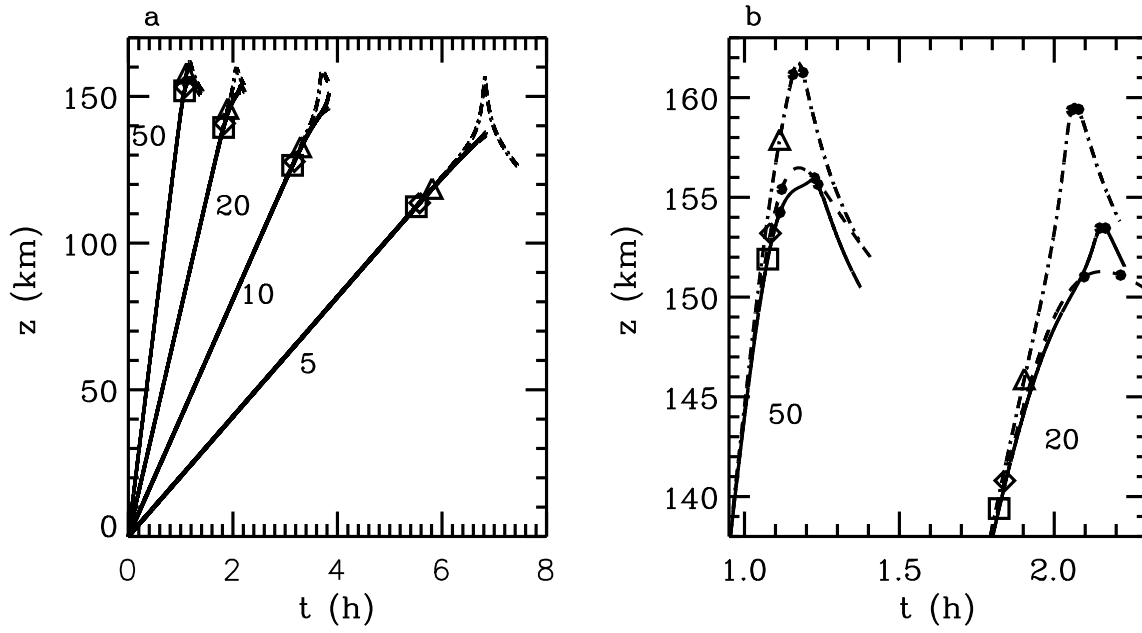


Figure 1:

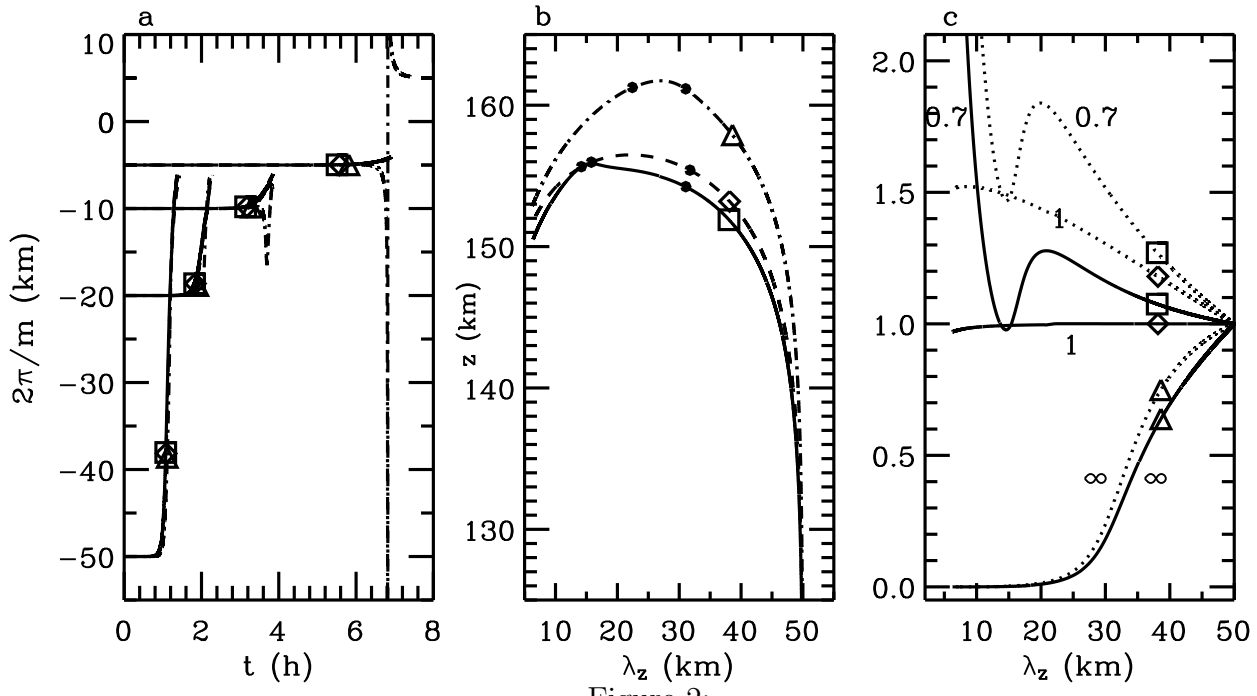


Figure 2:

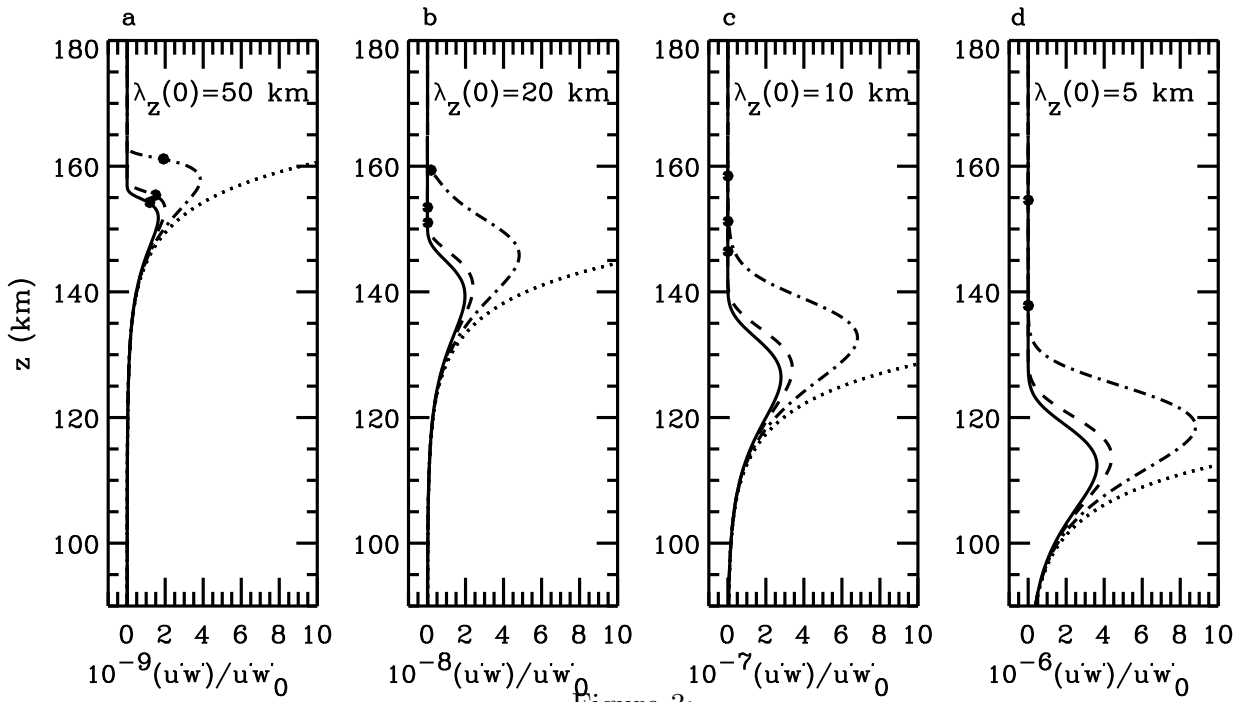


Figure 3:

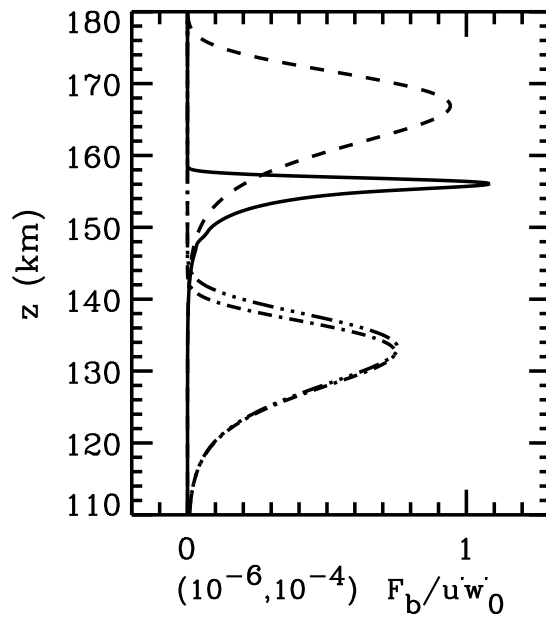


Figure 4: